Journal of Asian Earth Sciences 62 (2013) 180–204

Contents lists available at SciVerse ScienceDirect

Journal of Asian Earth Sciences

journal homepage: www.elsevier.com/locate/jseaes

Sedimentology and foreland basin paleogeography during Taiwan arc continent collision

Stefan Nagel [a,*], Sébastien Castelltort [a,b], Andreas Wetzel [c], Sean D. Willett [a], Frédéric Mouthereau [e], Andrew T. Lin [d]

[a] Department of Earth Sciences, ETH Zürich, Sonneggstrasse 5, 8092 Zürich, Switzerland
[b] Department of Earth Sciences and Environment, University of Geneva, Rue des Maraîchers 13, 1205 Genève, Switzerland
[c] Geological–Paleontological Institute, University of Basel, Bernoullistrasse 32, 4056 Basel, Switzerland
[d] Department of Earth Sciences, National Central University, 300 Jungda Road, Chungli, Taoyuan 101, Taiwan
[e] Université Pierre et Marie Curie, ISTEP, UMR 71934, Place Jussieu, 75252 Paris Cedex 05, France

ARTICLE INFO

Article history:
Received 9 March 2012
Received in revised form 20 August 2012
Accepted 3 September 2012
Available online 19 September 2012

Keywords:
Foreland basin
Taiwan
Paleogeography
Lithofacies
Sedimentary environment
Oblique collision

ABSTRACT

The Western foreland basin in Taiwan originated through the oblique collision between the Luzon volcanic arc and the Asian passive margin. Crustal flexure adjacent to the growing orogenic load created a subsiding foreland basin. The sedimentary record reveals progressively changing sedimentary environments influenced by the orogen approaching from the East. Based on sedimentary facies distribution at five key stratigraphic horizons, paleogeographic maps were constructed. The maps highlight the complicated basin-wide dynamics of sediment dispersal within an evolving foreland basin.

The basin physiography changed very little from the middle Miocene (~12.5 Ma) to the late Pliocene (~3 Ma). The transition from a passive margin to foreland basin setting in the late Pliocene (~3 Ma), during deposition of the mud-dominated Chinshui Shale, is dominantly marked by a deepening and widening of the main depositional basin. These finer grained Taiwan derived sediments clearly indicate increased subsidence, though water depths remain relatively shallow, and sedimentation associated with the approach of the growing orogen to the East.

In the late Pleistocene as the shallow marine wedge ahead of the growing orogen propagated southward, the proximal parts of the basin evolved into a wedge-top setting introducing deformation and sedimentation in the distal basin. Despite high Pleistocene to modern erosion/sedimentation rates, shallow marine facies persist, as the basin remains open to the South and longitudinal transport is sufficient to prevent it from becoming overfilled or even fully terrestrial.

Our paleoenvironmental and paleogeographical reconstructions constrain southward propagation rates in the range of 5–20 km/Myr from 2 Ma to 0.5 Ma, and 106–120 km/Myr between late Pleistocene and present (0.5–0 Ma). The initial rates are not synchronous with the migration of the sediment depocenters highlighting the complexity of sediment distribution and accumulation in evolving foreland basins.

1. Introduction

Foreland basins are mechanically coupled to orogens and store in their sedimentary archives most of the history of mountain building (Beaumont, 1981). The relationship between the tectonic evolution of a mountain range and sedimentation in its foreland has been extensively analyzed in different convergent basin systems around the world, e.g. Taiwan (Covey, 1984b; Teng, 1990), the Pyrenees (Burbank et al., 1992; Puigdefàbregas and Souquet, 1986), the European Alps (Allen et al., 1991) and the Himalayas (Burbank et al., 1988).

The Western foreland basin in Taiwan preserves an exceptionally detailed record of the Miocene–Pliocene–Pleistocene collision, exhumation and erosion of a young and active orogen (Fig. 1). The foreland basin infill comprises a 7–9 km thick succession of pre-orogenic and syn-orogenic Cenozoic strata (Lin and Watts, 2002; Lin et al., 2003; Yu and Chou, 2001). Geological and geophysical evidences suggest that part of this succession consists of siliciclastic facies that reflect the basin development from an early underfilled stage to a late steady-state stage. According to Covey (1986), mass balance calculations indicate a mismatch between sediment volume currently preserved in the basin and the amount of expected material eroded from the orogen since the onset of collision (based on an erosion rate of 5.5 km/Ma and a southward orogen area development since 3 Ma). Thus Covey (1986) suggested

* Corresponding author. Tel.: +41 446322365.
E-mail address: stefan.nagel@erdw.ethz.ch (S. Nagel).

1367-9120/$ - see front matter © 2012 Elsevier Ltd. All rights reserved.
http://dx.doi.org/10.1016/j.jseaes.2012.09.001

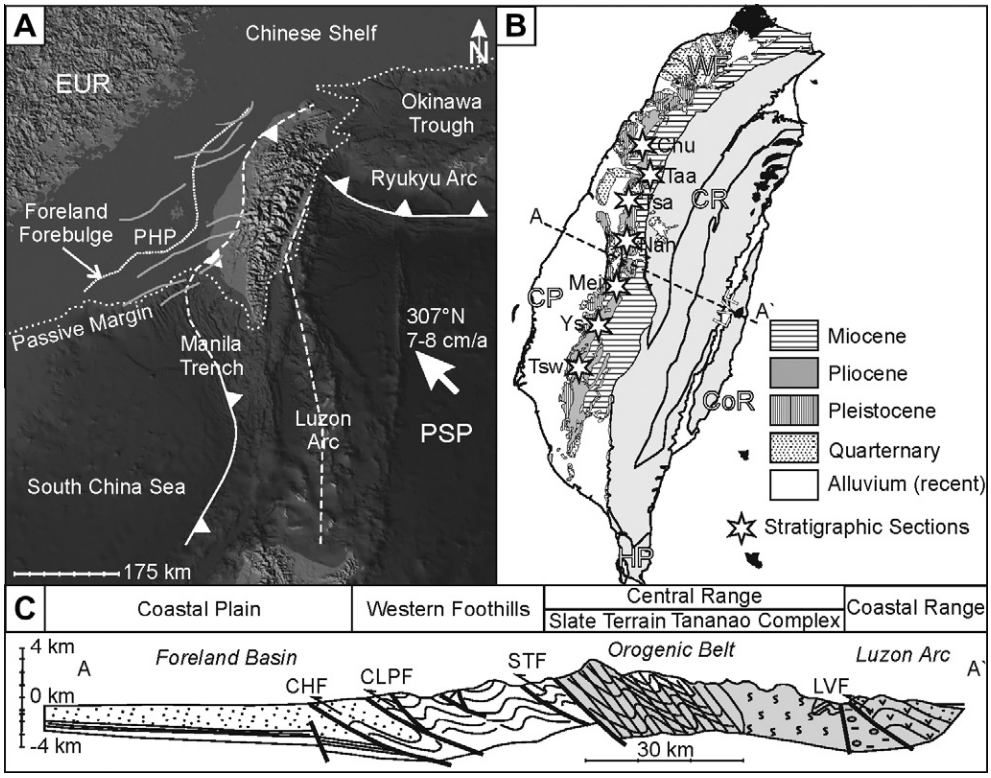

Fig. 1. (A) Plate tectonic configuration of the Taiwan area. The collision zone in Taiwan is divided into three main domains: Ryukyu arc-trench system and the associated Okinawa trough, an extensional basin as a result of the collision and subduction of the Philippine Sea plate; Luzon volcanic arc and Manila trench in the south; pre-collisional Eurasian continental shelf break. EUR = Eurasian continental plate, PSP = Philippine sea plate, PM = 200 m isobath (= recent shelf break), FF = foreland forebulge (Lin et al., 2003), PHP = Peikang High, (B) Geological provinces (Ho, 1988) and measured stratigraphic sections, CP = Coastal Plain, WF = Western Foothills, CR = Central Range, CoR = Coastal Range, HP = Hengchun Peninsula, LVF = Longitudinal Valley Fault, Chu = Chuhuangkeng, Taa = Taan River, Tsa = Tsaohuchi River, Nan = Nantou, Mei = Meishan, Ys = Yunshuichi, Tsw = Tsengwenchi and (C) Schematic cross section of Taiwan, CHF = Changhua fault, CLPF = Chelungpu fault, STF = Shuangtung fault (Teng, 1990).

that marine and fluvial processes "were efficient at transporting some of the debris out of the foreland basin, creating a basin of steady state size", which essentially resulted in maintaining shallow marine environment in the foredeep.

Numerous tectonic and sedimentary studies have addressed the progressive arc-continent collision (Barrier and Angelier, 1986; Chang and Chi, 1983; Chemenda et al., 2001; Covey, 1984a; Lin et al., 2003; Mouthereau et al., 2001; Sibuet and Hsu, 1997; Stephan et al., 1986; Suppe, 1981; Teng, 1990; Wang, 1987; Yu, 1993). Based on linear margin geometries Suppe (1981) first proposed that due to the obliquity between the PSP-EUR motion and the orientation of the Asian margin, the collision propagated southward at an average rate of 90 km/Myr with respect to the Luzon volcanic arc. In support of southward propagation of the collision, lithofacies analysis of the foreland basin filling shows a gradual southward deepening (Covey, 1984b), and rapid subsidence in the Southwestern part of the basin at 0.98 Ma (Hong, 1997), later than in the North (late Pliocene to early Pleistocene). In addition, isopach maps of the synorogenic series (Shaw, 1996) are indicative of a southward migration of the main foreland depocenters from late Miocene (6.5 Ma, e.g. Kueichulin fm.) to Pleistocene (1.1 Ma, e.g. Toukoshan fm.), however at an average rate of 31 + 10/−5 km/Myr (Shaw, 1996; Simoes and Avouac, 2006) much smaller than the predicted ~90 km/Myr.

This paper addresses how the southward propagation of the orogen is recorded in the sedimentary landscape evolution of the foreland basin of Taiwan. One major objective is to derive paleogeographic maps of the foreland basin at key time horizons in order to bring new constraints on the evolution of the southern propagation.

A detailed sedimentological and ichnological study of seven representative sedimentary sections in combination with literature data allows to distinguish sixteen facies grouped into seven facies associations. The sedimentary data form the base to propose a new facies model which incorporates modern data on waves from the Taiwan Strait as a means to calibrate paleobathymetry. Five facies maps were build for time slices at 12.5 ± 1.0 Ma, 5.5 ± 0.5 Ma, 3.5 ± 0.5 Ma, 2.0 ± 0.2 Ma and 0.5 ± 0.15 Ma.

These maps document the progressive shallowing of the Taiwan Strait with time as well as the progressive westward and southward migration of the coastline. The relatively slow (5–20 km/Myr) southward migration of the coastline is in agreement with depocenter migration, which demonstrates the strong control by mountain building and the related sediment dispersal system in this foreland basin on the distribution of paleoenvironments. These results add new constraints to kinematic models of plate collision in this area.

2. Geological and stratigraphic setting

The island of Taiwan is located at the plate boundary between the Eurasian plate (EUR) and the Philippine Sea plate (PSP, Fig. 1A). The PSP-EUR relative convergence velocity is of the order of 70–80 km/Myr (Seno et al., 1993) and leads to subduction of PSP beneath EUR along the Ryukyu arc trench system and opening of the Okinawa Trough backarc basin in the Northeast (Ku et al., 2009). The South China Sea is subducted along the Manila Trench, below PSP, in the West and South, which is accompanied by volcanism in the Luzon Arc. Collision of the Luzon volcanic arc (belonging to the PSP) with the EUR passive margin forms the Taiwan Mountains.

The geology of Taiwan is subdivided into four major tectonic-stratigraphic elements (Fig. 1B): The Coastal Plain (CP), the Western Foothills (WF), the Central Range (CR, Hsüehshan Range and

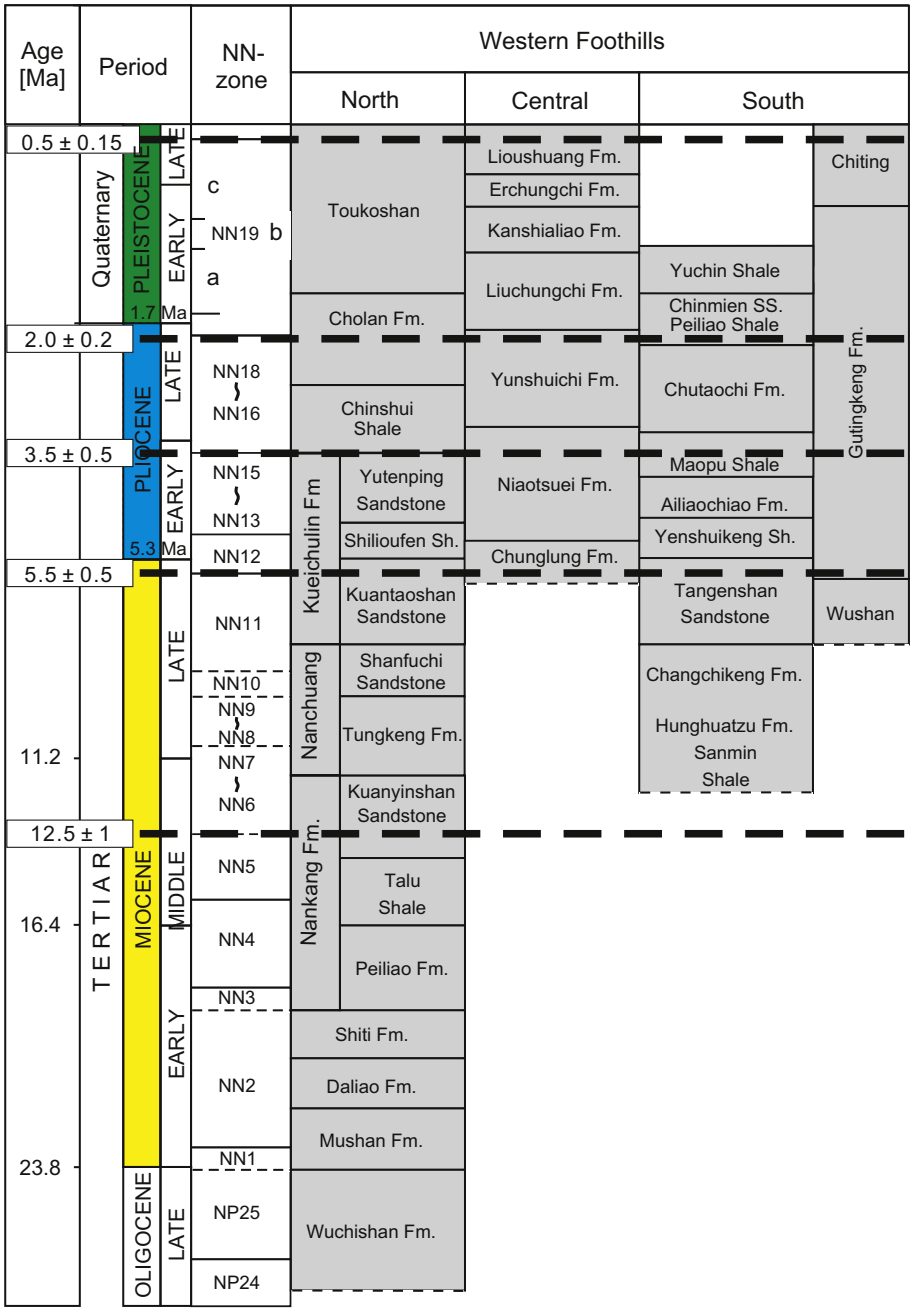

Fig. 2. Stratigraphic correlation of the Neogene sediments in the Western foreland basin from the northern, central (e.g. Peikang High) and southern part with biostratigraphic zonation used in this study (modified after Horng and Shea (2003)). The uncertainty of biostratigraphic ages depends on first and last appearance datum.

Backbone Range), and the Coastal Range (CoR). The Coastal Range is separated from the Central Range by the Longitudinal Valley Fault (LVZ). This zone is thought to represent the subaerial geological suture between the Philippine Sea plate and the Eurasian plate (Fig. 1) (Ho, 1988). The Coastal Range incorporates Neogene (22–5 Ma) rocks of the accreted Luzon arc (Dorsey and Lundberg, 1988). The area west of the Longitudinal Valley Fault (e.g. Central Range, Western Foothills and Coastal Plain) consists of metamorphic (Tananao complex and Slate terrain) and sedimentary rocks of the deformed continental margin (Teng, 1990). The Western Foothills (Fig. 2) form a fold-and-thrust belt built up of west-vergent thrusted Neogene clastic deposits of the modern foreland basin.

As a result of orogenesis and erosion, late Miocene to Pleistocene deposits with maximum thickness of up to 7–9 km have accumulated in the Western foreland basin (Lin et al., 2003). They record infill from both the Chinese Mainland in the West as well as from the emerging Taiwan island to the East.

Most authors suggest that the onset of arc-continent collision took place during late Miocene, between 12 and 8 Ma (Chang and Chi, 1983; Huang, 1984; Tensi et al., 2006) and late Pliocene, between 5 and 2 Ma (Dorsey and Lundberg, 1988; Pelletier and Stephan, 1986; Suppe, 1980, 1988; Teng, 1990). Seismic reflection profiles from the offshore Taiwan Strait show a distinct unconformity separating onlapping foreland basin sequences above from passive margin sequences below; they are interpreted as the flexural forebulge unconformity marking the displacement of subsidence in front of the moving orogen (Yu and Chou, 2001). This unconformity represents the boundary between the pre-collisional Nanchuang fm. and the syn-collisional Kueichulin fm. and was estimated approximately 6.5 Ma (Fig. 2, Lin et al., 2003).

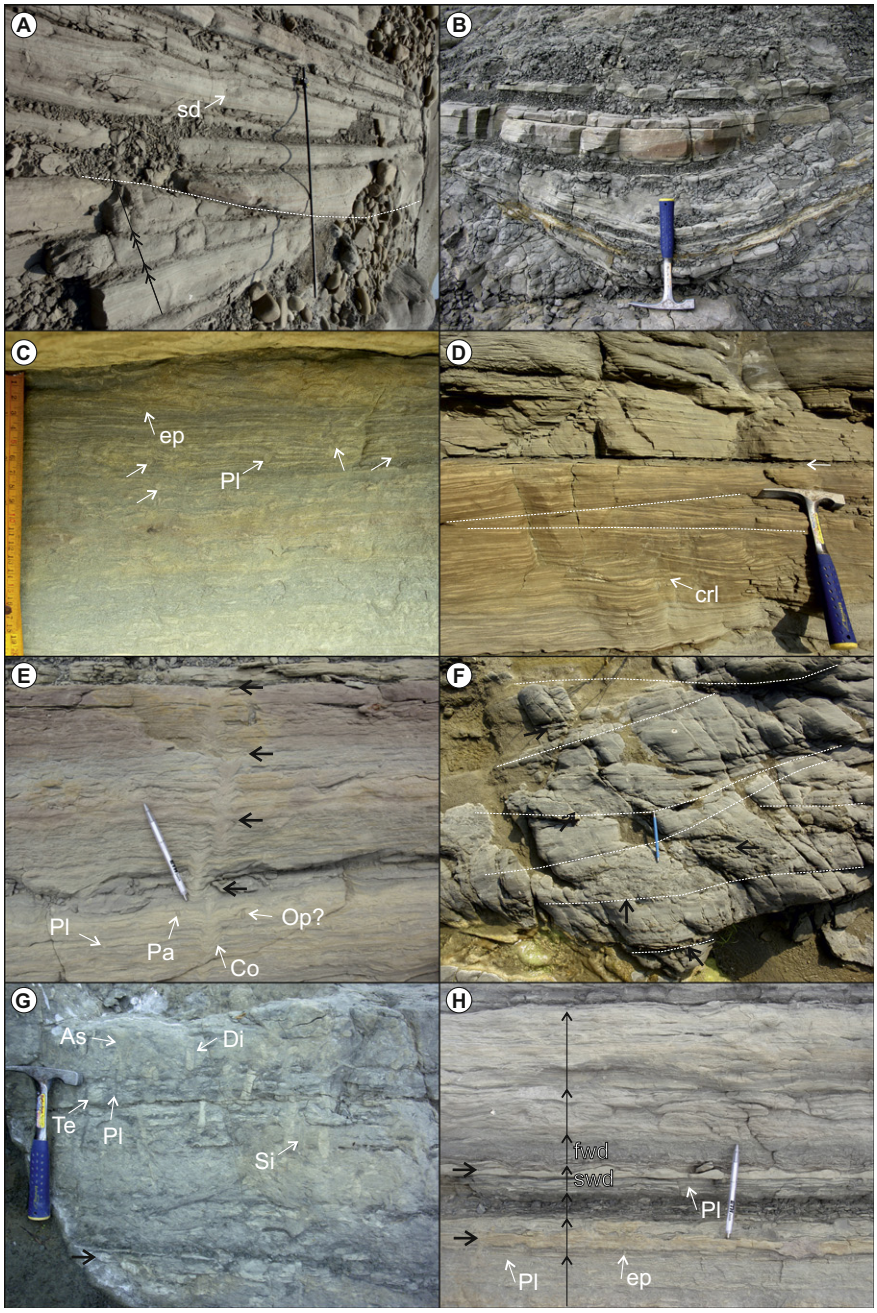

Fig. 3. (A) Sandy delta-front deposits in the proximal upper offshore. Fine, laminated silty sandstones separated by thin mud layers (black arrows); abundant soft sediment deformation structures in the upper part (sd). The sandstone bed in the middle reveals low angle shallow scours several meters broad, but only a few tens of decimeters deep, probably generated by longshore currents and/or storm surge currents (dashed line). Only trace fossil *Chondrites* occurs. Chutouchi formation, Tsengwen-chi, Zu-Malai-Farm. (B) Several episodes of infill of a small channel in the lower offshore. The siltstones are finely laminated and separated by mud layers deposited during quiet periods. The low angle scour-and-fill and uniform fine grain size suggest relatively low energy environment. Top Chinshui Shale, Meishan section. (C) Intense bioturbation in delta front deposits in the upper offshore realm almost obliterate primary sedimentary structures. Low diversity trace fossil suite of *Planolites* (Pl) with abundant escape traces (ep) and rare synaeresis cracks, suggesting flood emplacement. Ailiaochiao formation, Tsengwen-chi, Toll Station. (D) Storm-dominated deposition in the delta front, upper offshore. Facies is similar to C, but with increased energy during deposition. Note the low-angle cross bedding and climbing ripples (crl), suggesting a strong unidirectional flow during deposition (dashed lines). The two units are separated by a 2 cm thick mud layer deposited during fair-weather conditions (arrow). Trace fossils are virtually absent. Ailiaochiao formation, Tsengwen-chi, Toll Station. (E) Same facies as in C. Delta front in the upper offshore characterized by continuous rates of deposition. Several events of colonization and adjustment of *Conichnus* (Co). Trace fossils include *Planolites* (Pl), *Palaeophycus* (Pa) and probably *Ophiomorpha* (Op). *Tasselia* and *Bergaueria* were commonly observed together with *Conichnus* (not shown). Former sediment surfaces marked by black arrows. Ailiaochiao formation, Tsengwen-chi, Toll Station. (F) Storm event deposition in the upper offshore. The amalgamated sandstones show large scale hummocky cross stratification and mud pebble conglomerates (black arrows) in the swales. Note that the following storm events erode into the underlying beds. Ailiaochiao formation, Tsengwen-chi, Toll Station. (G) Thoroughly bioturbated fair-weather deposits at the proximal end of the upper offshore. Trace fossil suite contains *Teichichnus* (Te), *Planolites* (Pl), *Siphonichnus* (Si), *Asterosoma* (As) and *Diplocraterion* (Di). Note the completely obliterated storm sand layer (black arrow), in parts with *Ophiomorpha*. Top Chinshui Shale, Tsaohu-chi section. (H) Wave dominated delta front in the proximal upper offshore. The sharp based storm sand layer (swd) in the middle shows asymmetrical current ripples indicating flow to SW (black arrow). On top aggrading, relatively steep climbing ripples due to rapid sedimentation (e.g. suspension fall-out), indicated by rare escape traces (ep). On top mud-dominated thoroughly bioturbated fair-weather deposit (fwd). The succession shows strong, (probably seasonal) stratification as previously analyzed by Castelltort et al. (2011) in the synchronous Kueichulin formation to the North (Meishan section). Different cycles of sedimentation based on sedimentary structures, grain size and trace fossils indicated by vertical arrows. Ailiaochiao formation, Tsengwen-chi, Toll Station.

Geographically the foreland basin fill is found in the Western Foothills, the Coastal Plain and the Taiwan Strait offshore (Fig. 1). The northern part of the foreland basin fill is dominated by shallow marine (e.g. deltaic) and non-marine (e.g. braided rivers) sand-dominated deposits, whereas the southern part is dominated by deeper marine mud-rich deposits (Covey, 1984a). The facies differentiation has been ascribed to the subsidence pattern varying due to the moving tectonic load in front of the growing accretionary wedge (Covey, 1986) and separation of the northern and southern part by the Peikang High (Chou, 1973; Tang, 1977). In addition, the development of the foreland basin system was influenced by the underlying inherited basement structures that formed during Paleogene rifting of the Asian passive margin (Lin et al., 2003).

2.1. Stratigraphic framework

Temporal and spatial changes in sedimentary facies are expressed by distinguishing various formations from north to south. The studied Neogene sequences (12.5–0.5 Ma) crop out in the Western Foothills along the strike of the mountain range (Fig. 1). The biostratigraphy of these series has been extensively analyzed (Chang and Chi, 1983; Horng and Shea, 1996; Huang and Huang, 1984). Biostratigraphic correlation of the formations from North to South in Taiwan is synthesised in Fig. 2. The syn-collisional sedimentary sequences are similar from north to south and were first described by Covey (1984a) in the context of foreland basin evolution.

The upper Miocene units (e.g. Nanchuang and lower Kueichulin formation) are tidally-influenced shallow marine sediments. In the Northwestern part of Taiwan, these units are poor in marine fossils but contain abundant plant debris suggesting a coastal to shallow-marine origin (Chou, 1973). Towards the southwest, the Nanchuang formation gets gradually enriched in marine fossils. The grain size of Miocene sandstones decreases from North and Northwest towards South and Southeast indicating the general transport direction during this time (Chou, 1973).

The Nanchuang formation is unconformably overlain by the late Miocene to Pliocene Kueichulin formation. The latter consists mainly of shallow marine tide-influenced deltaic deposits. To the south, the time-equivalent of the Kueichulin formation is the mud-dominated lower Gutingkeng formation which is of deeper marine origin (e.g. lower offshore).

Above the Kueichulin formation, the up to 300 m thick mid-Pliocene Chinshui Shale is composed of mudrocks; it is interpreted to record a period of maximum flooding in the history of the foreland. Reworked fossils and paleocurrent directions indicate that the main source of the sediment at this period was the Taiwan orogen to the East (Chang and Chi, 1983).

The late Pliocene and early Pleistocene Cholan formation progrades onto the Chinshui shale and comprises wave and tide influenced deltaic deposits progressively dominated by fluvial processes, with a general decrease in grain size southward towards silt and shale. The formation is rich in slate fragments derived from the Paleogene slate terrain in the East (Chou, 1973).

Above the Cholan formation, the final regressive stage ends with the deposition of the coarse grained sandstones and conglomerates of the Toukoshan formation, interpreted as braided rivers and alluvial fan deposits (Covey, 1984a, 1986) sourced in the orogen to the East.

3. Sedimentology of foreland series

3.1. Previous studies of depositional environments

The general paleocurrent direction from north to south during the Miocene-Pleistocene resulted in the deposition of coarse fraction in a (inner) shelf environment in Northwestern Taiwan (Chou, 1970), whereas most of the fine fraction was transported to the south (over the Peikang basement High) and deposited in deep neritic to shallow bathyal environment (Chou, 1980). The Northern part was analyzed in detail by numerous studies mainly focusing on the Miocene sedimentology (Chiu, 1975; Chou, 1972, 1973; Yeh and Yang, 1994) and biostratigraphy (Huang, 1976a).

The Miocene successions in the Northwestern part are dominated by fluvial, deltaic and inner neritic environments (Chou, 1970). Isopach maps show an increase in thickness from the Northwestern part towards the South and a source area in the West and Northwest, respectively (Chang, 1971). More recent studies focused on linking the shallow marine, deltaic to tidal deposits in the North to relative sea level changes and stated the major influence of global eustacy on these Miocene sediments (Yu et al., 1999). The central part, e.g. the Peikang basement high, shows a wide range of depositional environments, including beach deposits, shoreface, continental shelf and slope, as well as submarine fan deposits (Chiu, 1972; Yeh and Yang, 1994). In fact, seismic profiles correlated with wells in the central part of Taiwan display several paleo-canyons of early Pliocene to Pleistocene age (Fuh et al., 1997). High-resolution sedimentological analyses reveal the large influence of tectonics and high-frequency sea level fluctuations in the central part (Chen et al., 2010; Chen and Liu, 1996; Yeh and Yang, 1994).

Several studies in the Southwestern part of Taiwan, namely along the Nantzuhsien and Tsengwen-chi sections, show deposition in offshore environments for most of the time (Chen et al., 2001; Ting et al., 1991; Yu et al., 2008) with abundant (erosional) unconformities. Paleobathymetry was estimated in the Southwestern part of Taiwan using the ratios of planctonic and benthonic foraminifera (Chow, 1980). These ratios were calibrated with recent foraminifera data from the Taiwan Strait and provided water depths of 40 to 80 m for the upper Miocene (Kueichulin fm. equivalent), 175–200 m for the lower Pliocene (Chinshui fm. equivalent), 200–220 m for the upper Pliocene (Cholan fm. equivalent) and 30–60 m for the Pleistocene (Toukoshan fm., Chow, 1980). Additional information is provided by paleoenvironmental studies of the Chinshui Shale, Cholan and Toukoshan formations in the Central part of Taiwan using ostracodes. They demonstrate that ostracodes from the Chinshui Shale were deposited in shallow marine warm water close to the shoreline with high deposition rates (Hu and Yang, 1975), and that the environmental setting changed little from Chinshui to Cholan and Toukoshan (Hu, 1976). Comparison of the ostracodes from the Toukoshan formation with recent ostracodes show that they accumulated in water depth of about 20 m in average (Hu, 1977).

Covey (1984b) analyzed the spatial distribution of depositional environments in the foreland basin and reconstructed the filling history. The offshore marine assemblage formed below storm wave base, e.g. probably deeper than 200 m water depth. The shallow-marine assemblage contains sedimentary structures suggesting a similar depositional environment to the present day Taiwan Strait. It differs from deltaic and non-deltaic deposits by the less coarse grained sandstones and the lack of associated non-marine strata. The youngest deposits were dominated by fluvial systems, e.g. cobble-dominated rivers and sandy fluvial deposits. In summary, Covey (1984a) showed that the Southern part of the basin was dominated by offshore marine assemblages, whereas the Northern part mainly contains shallow marine, deltaic and fluvial assemblages.

3.2. Paleobathymetric profile

The depositional pattern encountered in the foreland basin of Taiwan (description below) is suggestive of the classical

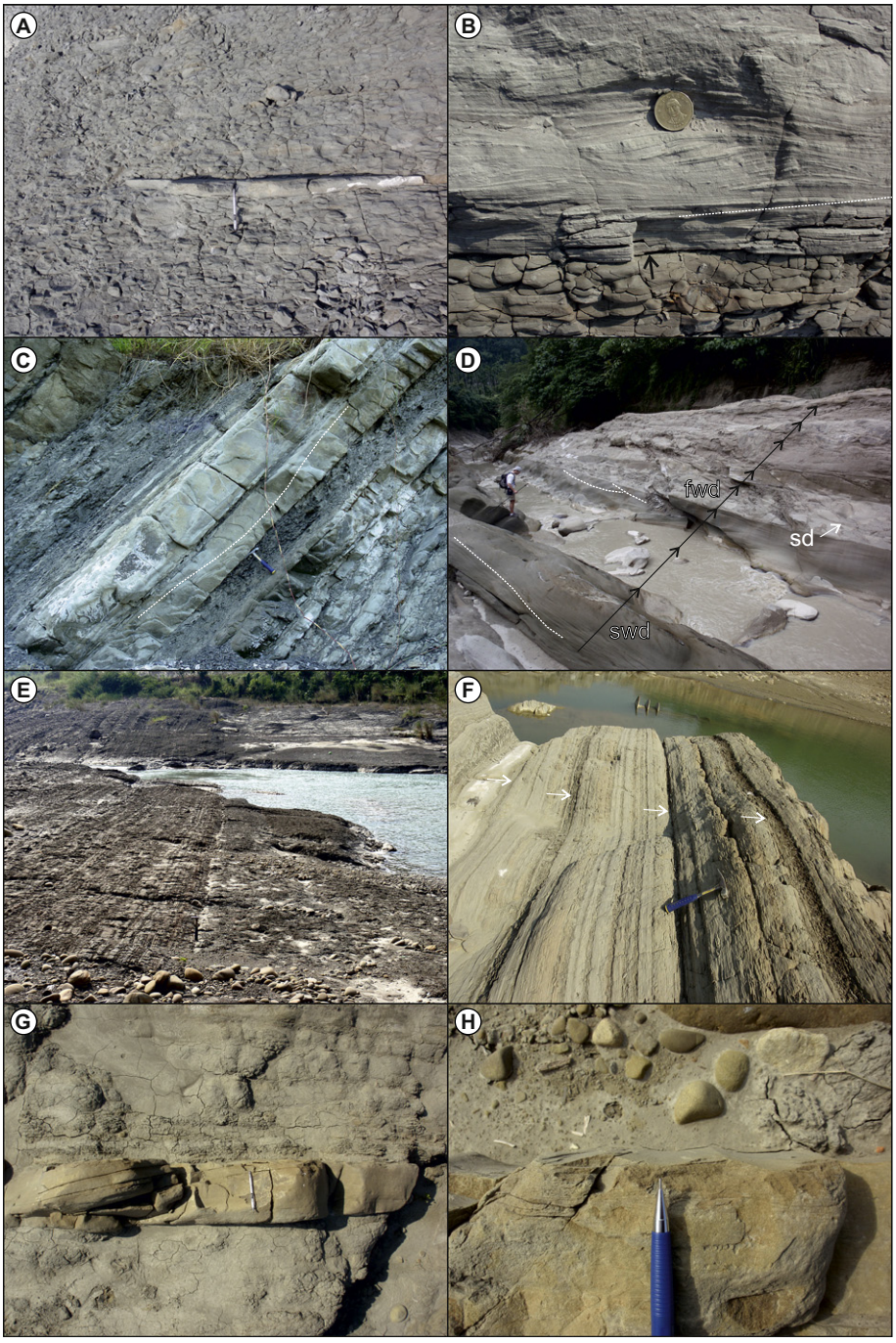

Fig. 4. (A) Distal storm bed in the upper offshore. The fine sandstone is laminated, with micro-hummocky cross-stratification. Top parts are slightly bioturbated with *Nereites* and *Helminthopsis*. Maopu Shale, Tsengwen-chi, Zu-Malai-Farm. (B) Exceptional storm event in the mud-dominated lower offshore. Massive mudstone (bottom) is sharply cut by silty to sandy mud layer (black arrow) with low-angle climbing ripples. The low-angle of climb suggests a strong unidirectional flow to the left (NE). Ailiaochiao formation, Tsengwen-chi, Zu-Malai-Farm. (C) Several storm sand layers separated by structureless mud layers, deposited in the distal upper offshore. The sandstones show large scale hummocky cross-stratification (dashed line), are sharp based and are not burrowed. On top thoroughly bioturbated fair-weather deposits. Top Chinshui Shale, Tsaohu-chi Section. (D) Large scale hummocky-cross stratified sandstones (indicated by dashed lines) and slumped mudstone layers (sd), upper offshore. Bioturbation virtually absent, with rare post-storm colonization by *Ophiomorpha* and *Palaeophycus* producers. fwd = fair-weather deposition, swd = storm weather deposition. Niaotsui formation, Yunshui-chi section. (E) Massive mudstone, lower offshore (right) and distal upper offshore (Prodelta) on the left. Chutouchi formation (left) and Maopu Shale (right), Tsengwen-chi, Zu-Malai-Farm. (F) Wavy to lenticular bedded silty mudstone in the distal upper offshore. Interval shows no bioturbation. Note the rhythmic occurrence of thick (ca. 5–10 cm) massive mud layers (arrow), suggesting either tidal and/or seasonal influence. Base Ailiaochiao formation, Tsengwen-chi, Toll Station. (G) Fine-grained sandstone bed showing well developed hummocky cross-stratification, distal upper offshore, Tsengwen-chi, Zu-Malai-Farm. (H) Wave-influenced storm sand, proximal upper offshore. The ripples are symmetrical and sharp crested indicating deposition close to the fair-weather wave base. Liuchungchi formation, Tsengwen-chi, Zu-Malai-Farm.

proximal–distal facies distribution related to the influence of waves and tides (Fig. 8).

In the present study, a major specificity of Taiwan is taken into account in addition: the important influence of typhoons. Therefore, the typhoon wave base (or maximum storm wave base) is defined that refers to heavy storms during summer (from June to October). Then southwest monsoon prevails and 4–6 typhoons hit the island with maximum wind speeds and induce long-period

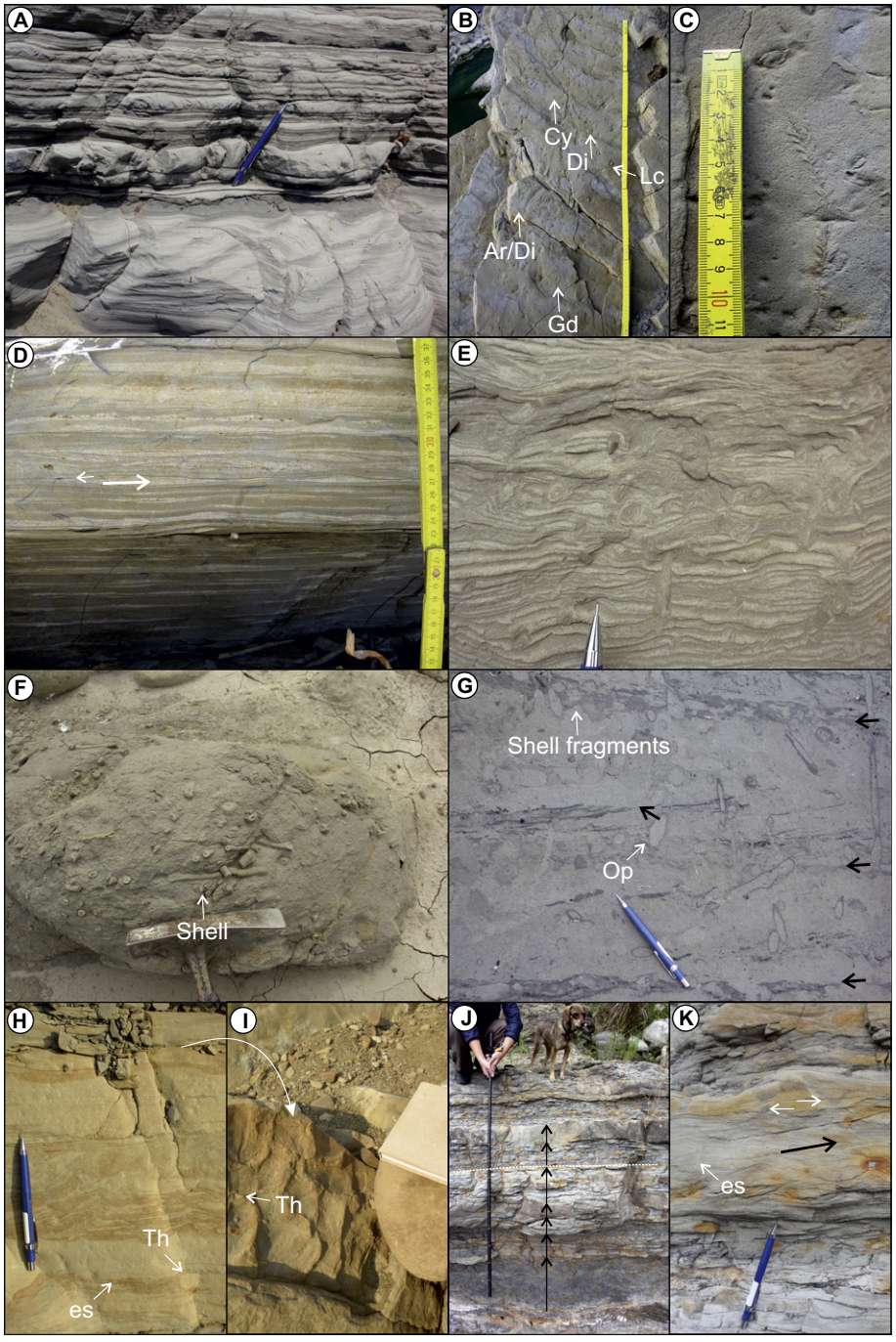

Fig. 5. (A) Wavy and planar laminated silty mudstones and fine sandstones, lower shoreface. Recurrent pattern of sand-mud couplets imply tidal influence. Lower unit shows climbing ripple lamination. Bioturbation is low to absent, commonly restricted to a distal *Cruziana* ichnofacies. Yutengping Sandstone Mb. (Kueichulin fm.), Meishan section. (B) Trace fossil association in the heterolithic wavy bedded facies of (A). *Nereites* (Ne), *Gordia* (Gd), *Lockeia* (Lc), *Protovirgularia* (P), *Diplocraterion* (Di) or *Arenicolites* (Ar), *Cylindrichnus* (Cy). (C) Close-up view of *Protovirgularia* trackway. Yutengping Sandstone Mb. (Kueichulin fm.), Meishan section. (D) Lenticular bedded muddy siltstone with small bidirectional current ripples (arrows), dominant current direction to the right (SW). Rip-up mud pebbles aligned or imbricated on basal surfaces. Delta front, lower shoreface. Yutengping Sandstone Mb. (Kueichulin fm.), Meishan Section. (E) Intensely bioturbated heterolithic laminated facies in the lower shoreface. *Planolites*, *Cylindrichnus*. Top Yutengping Sandstone Mb. (Kueichulin fm.), Meishan section. (F) Bioturbated massive silty mudstone with abundant *Schaubcylindrichnus* and shell debris (arrow), lower shoreface. Ailiaochiao formation, Tsengwen-chi, Toll Station. (G) Intensely bioturbated fine to medium grained sandstone with cross bedding and scattered shell debris, middle to upper shoreface. Note the three completely bioturbated mud layers occurring between the cross-bedded sandstones (black arrows). Background consists of intense but indistinct mottling of mostly incomplete light patches. Common trace fossil is *Ophiomorpha* being similar to the *Ophiomorpha-Planolites* ichnofabrics of Pollard et al. (1993). Episodic high-energy events are indicated by erosion of underlying cross-beds (middle, black arrow). Cholan formation, Dahan-chi Section. (H) Wavy and parallel laminated massive fine sandstone and muddy siltstone with interference ripple lamination on top (Picture I), proximal delta front, lower to middle shoreface. Bioturbation is low with abundant escape structures (es) and distorted bedding. Ailiaochiao formation, Tsengwen-chi, Toll Station. (J) Storm- and wave-dominated heterolithic climbing ripple-laminated sandstone with little muddy drapes and silty mudstone interlaminations. These often overlie structureless mudstone and wavy to lenticular bedded facies. Interspersed fine laminated sandstones with cross-bedding are interpreted as storm deposits, middle to upper shoreface. Taan-chi section. (K) Close up of (J). Sand dominated climbing ripple lamination (black arrow) with bidirectional current ripples (white arrows) on top. Bioturbation is low to absent, only few escape structures (es). Kuantaoshan formation, Taan-chi section.

and high-amplitude waves (Jan et al., 2002; Wang, 2004). The normal storm wave base (or minimum storm wave base), in contrast, refers to average winter storms (from October to May) with strong and constant Northeast directed winds. Winter storms show in general regular occurrence, frequency and duration, whereas summer conditions are more variable and punctuated by typhoons (Zhang, 2002).

The water depth of the typhoon and minimum storm wave base was calculated by using modern wave data from the Taiwan Strait recorded at 5 stations on the west coast during the last 3 years (http://www.cwb.gov.tw/eng/index.html). The wave data consist of monthly averaged wave height and wave period and the maximum wave height and period recorded during observation (Fig. 9). Fair-weather conditions were associated with mean wave height and period, whereas the maximum wave height and period were assigned to storm conditions. Calculated values during the months June to October were attributed to typhoons.

The calculation is based on physical principles of sediment movement under oscillatory wave motions (Komar and Miller, 1973) which allow an estimation of the water velocity required to move sediment of a certain grain size (competence velocity) at a given water depth. The grain size was determined by examining thin sections from hummocky cross-stratified storm sand layers (Fig. 4G). A grain size between fine sand and silt (3–4° ϕ) describes sufficiently well the diversity of our samples and agrees well with the analysis of characteristic winter storm data in the East China Sea, where fine grained material (e.g. fine sand and silt) can be put in suspension at water depths of up to 100 m (Graber et al., 1989).

The modern seasonal variation of the wave base is well shown by this data (Fig. 9). It demonstrates that occasional high amplitude events such as typhoons clearly have the capacity to generate substantial resuspension of the sediment across most of the Taiwan shelf.

The modern Typhoon storm wave base is situated at an average water depth of 100 m in a range of 50–140 m. A normal winter storm mobilizes fine sand and silt at an average water depth of 60 m in a range of 30–90 m. The fair weather conditions are best described by a fair weather wave base of 15 m in a range of 10–20 m. By analogy with modern conditions these values were applied to the facies encountered in Taiwan.

These estimates are in agreement with studies from the East China Sea and New Zealand which show that storm waves are capable to resuspend sediments in water depth of 50–100 m (Graber et al., 1989; Manighetti and Carter, 1999). Theoretical calculations of wave induced bottom currents and bed shear stresses in the Yellow Sea also demonstrate that typhoons have the potential to erode sediment in water depth up to 90 m (Booth and Winters, 1991).

Furthermore a tide-related facies zonation including subtidal, intertidal and supratidal settings was considered. Today, the semidiurnal tide is dominant in the Taiwan Strait with a mean tidal range at the Northwest tip of Taiwan higher than 4 m while at the Southeast tip is lower than 1 m (Lin et al., 2001).

The partitioning of the depositional profile follows the shoreface model suggested for the Cretaceous Western Interior basin by Pemberton et al. (1992), but adjusted to Taiwan. The lower offshore represents a-mud dominated environment below the maximum storm wave base (below typhoon influence). The upper offshore environment lies in between minimum storm wave base and mean fair-weather wave base (Fig. 8). The shoreface starts from the mean fair-weather wave base to the mean lower tidal range (Fig. 8). The transition from lower shoreface to upper shoreface is subtle, but usually marked by increasing occurrence of well sorted sandstones (shoaling wave zone). The foreshore environment is located completely within the intertidal regime and it is followed by the backshore (e.g. supratidal or fluvial) environment.

3.3. Lithofacies description and interpretation

Several stratigraphic sections in the Western Foothills were studied in detail (Fig. 1B). They follow a north–south directed transect that delivers insight into the variation of depositional environments in front of the growing orogen. The facies pattern of five time horizons were addressed, before, around and after the time of initiation of foreland basin subsidence in late Miocene to middle to late Pleistocene (Chi and Huang, 1981; Ho, 1988; Lin et al., 2003; Teng, 1990; Tensi et al., 2006). Data from seven sections (see Fig. 1B for location) were collected and analyzed on the basis of sedimentary texture and structure, nature of bedding and bedding contacts, trace fossil content (intensity and distribution), and lateral variability. The sections are localized in the Chuhuangkeng anticline on the Houlong-chi, on the Ta'an-chi, on the Tsaohu-chi, on the Jhangping-chi and Pinglin-chi (Nantou), in the Jioucyongping syncline of the Meishan area, on the Yunshui-chi, Chiayi and in the Yujing syncline on the Tsengwen-chi.

In the Miaoli area, the Houlong-chi section is situated in the Chuhuangkeng anticline and was previously described by Huang (1976b) and Covey (1984a) among others. It covers partially the Nanchuang and Cholan formation.

The Ta'an-chi section preserves the lower Kueichulin formation (e.g. pre- to syn-collisional facies). Here, the uppermost part (e.g. Toukoshan fm.) was already described by Covey (1984a).

The stratigraphy of the Tsaohuchi-section was recently analyzed by Chen et al. (2001), using magnetostratigraphy from the Chinshui Shale (middle Pliocene) to the Toukoshan fm. (Pleistocene).

Near the city of Nantou, the Jhangping-chi section shows the transition from shallow marine deltaic sedimentation (Cholan fm.) to a fluvial-influenced depositional environment (Toukoshan fm.).

The same succession was also described in the Chungkungliao section by Covey (1984a), the Pinglin-chi section southwards (Chou, 1971) and the Miocene strata more to the East by Chiu (1972).

The Meishan section shows the transition from the last stage of the Kueichulin formation in the middle Pliocene (Yutengping Sandstone Member) to late Pliocene (Cholan fm.). The section was first described and analyzed by Castelltort et al. (2011).

The Yunshui-chi section shows upper Miocene to lower Pleistocene series (Chunglun fm. to Kanshaliao fm.) of storm dominated sediments (Wu and Wang, 1989).

The Tsengwen-chi section was extensively studied in the past by several authors (Chen et al., 2001; Chi, 1978; Chung, 1968; Hong, 1997; Lee et al., 1990) and thus, biostratigraphic and magnetostratigraphic data as well as an analysis of the depositional environments in the Southern part of Taiwan are available from literature.

The lithofacies are briefly outlined in Table 1; sixteen lithofacies were indentified that then were grouped into seven lithofacies associations. In Table 1 they are numbered having the lithofacies association as first number followed by the lithofacies. The main lithofacies associations match well a wave and tide dominated zonation consisting of lower offshore, distal upper offshore and prodelta, proximal upper offshore and delta front, lower shoreface, upper shoreface, foreshore and backshore. The identified facies are described and interpreted below. The facies encountered in the sections are shown in Fig. 10.

3.3.1. Lower offshore

The lower offshore is characterized by high mud content. Strata with increased silt-content may show very fine (sub-) millimeter-scale lamination (F1.1). Dark massive mudstone layers (F5.3) and cm-thick lenticular bedded layers (F1.1) are often interbedded

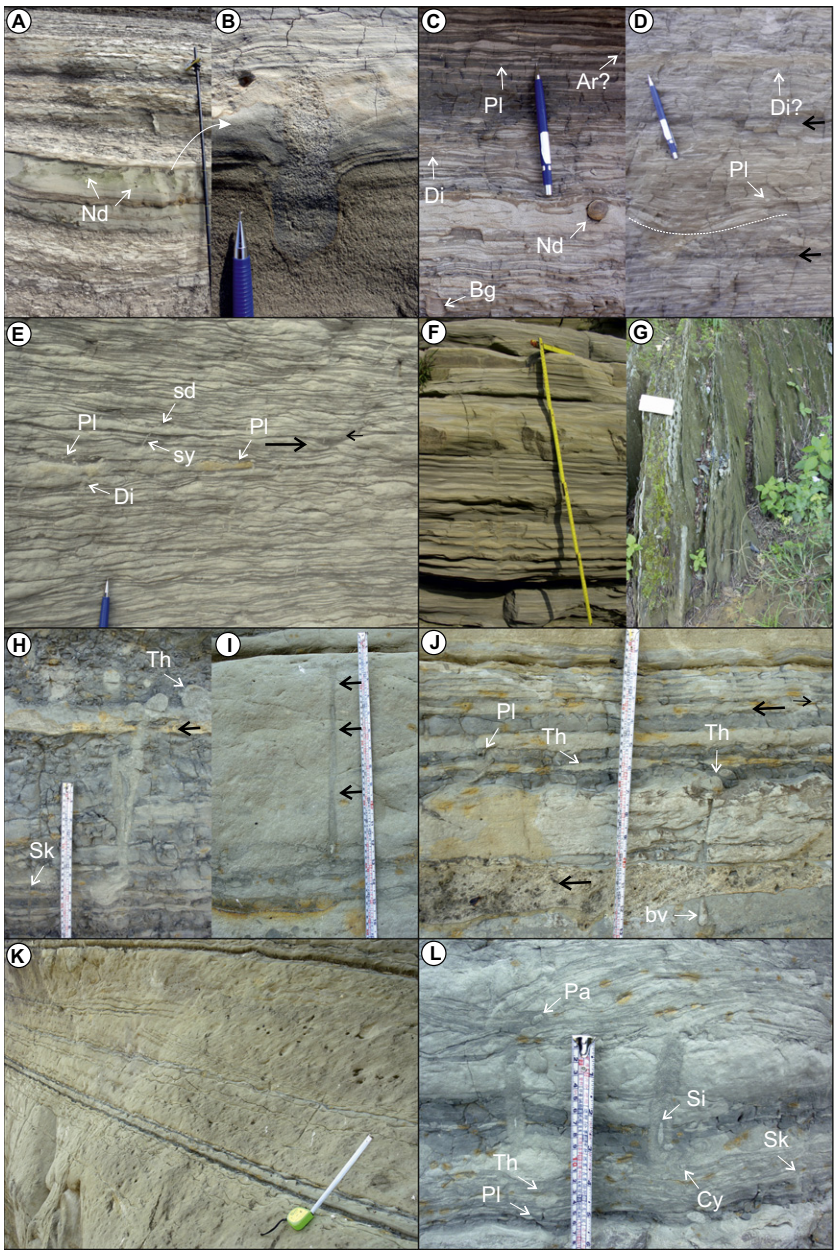

Fig. 6. (A) Wave- and tide-dominated upper shoreface facies, consisting of alternating of millimeter to centimeter-thick wavy and lenticular bedded mud and fine-grained sand layers. Massive laterally extent medium-grained sandstone beds deposited during storm events. Burrows are abundant, but low diverse. Sand beds contain abundant iron sulfide nodules (nd) resulting from reducing conditions in an organic-rich environment. Dahan-chi section. (B) Close up view of (A). The top surfaces (arrow) of the storm sand layers contain abundant *Conichnus* (Co) and in parts *Diplocraterion* (Di). Nanchuang formation, Dahan-chi section. (C) Wavy- and lenticular-bedded mudstone and interlaminated sandstones with abundant iron sulfide nodules (nd), tide-dominated upper shoreface. Note the rhythmic variation of mud- and sand-dominated layers due to tidal influence. Bioturbation is intense displaying a diminished *Skolithos* suite, *Planolites* (Pl), probably small *Arenicolites* (Ar) and *Diplocraterion* (uncertain since no horizontal cuts were found). Bottom shows a vertical unlined burrow with rounded base attributed to *Bergaueria* isp. (Bg). Nanchuang formation, Dahan-chi section. (D) Thinly, rhythmic, wavy- and lenticular-laminated siltstones and mudstones, middle to lower shoreface. Weak tidal influence is indicated by darker muddy intervals, probably monthly or annual cycles (black arrows). Burrows are commonly sparse, *Diplocraterion* (Di), *Planolites* (Pl). Note the small channel-like scours (dashed line). Nanchuang formation, Dahan-chi section. (E) Sand dominated wavy- and lenticular-bedded mudstone and sandstones with bidirectional current ripples (black arrows). The increased proportions of sandstone beds with combined interbedded oscillatory and current structures suggest a rather proximal sedimentation within the upper shoreface regime. Dominant flow direction is to the right, with a weak flow component to the left aggrading on top of the dominant current ripples, both separated by a thin mud layer. Thin distorted areas (sd) and synaeresis cracks (sy) are visible. Facies is similar to vertical polychaete dwelling traces (*Skolithos*, *Trichichnus*) found in estuarine environments (Buatois et al., 2005). Nankang formation, Chuhuangkeng section. (F) Rhythmically layered wavy sandstones draped by lenticular silty mudstones. Bidirectional current ripples to opposite directions are included in the fine-grained drape. The ripples are predominantly oriented towards the W–SW. Note two equilibrium traces *Siphonichnus*. Yutengping Sandstone, Meishan section. (G) Tangential cross-bedding with mud drapes on the foresets and nearly symmetrical ripples with weak flow direction to the NW (N310). The cross beds point to S–SE. Subtidal, upper shoreface. Cholan formation, Chuhuangkeng section. (H) Bioturbated wavy- to lenticular-bedded mudstones with medium to coarse (storm) sand layer (black arrow), lower to middle shoreface. The sand layers contain abundant organic material. Dwelling structure of a suspension-feeding bivalve, ca. 30 cm in length, further trace fossils include *Skolithos* (Sk) and *Thalassinoides* (Th). Base Yutengping Sandstone Member, Taan-chi section. (I) Equilibrium structure of a bivalve with three re-adjustments (black arrows) to the former sediment surface, upper shoreface. Base Yutengping Sandstone Member, Taan-chi section. (J) Completely bioturbated mudstone (base of picture) covered by medium-grained sandstone with cross-stratification and abundant coarse organic matter (black arrow). On top flaser-bedded sandstone with wave ripples and rhythmically layered mudstone and sandstone with bidirectional current ripples. Trace fossil suite consists of *Planolites* (Pl), *Thalassinoides* (Th), bivalve (Bv). Storm- and tidal influenced upper shoreface. Yutengping Sandstone Member, Taan-chi section. (K) Follows on top of (J). Large-scale subtidal foresets with symmetrical wave ripples. The foresets thin laterally and are separated by mud drapes. Subtidal, upper shoreface. Yutengping Sandstone Member, Taan-chi section. (L) Completely bioturbated wavy- to lenticular-bedded silty mudstone, lower shoreface. Mixed *Skolithos–Cruziana* ichnofacies with *Palaeophycus* (Pa), *Siphonichnus* (Si), *Skolithos* (Sk), *Cylindrichnus* (Cy), *Thalassinoides* (Th), *Planolites* (Pl).

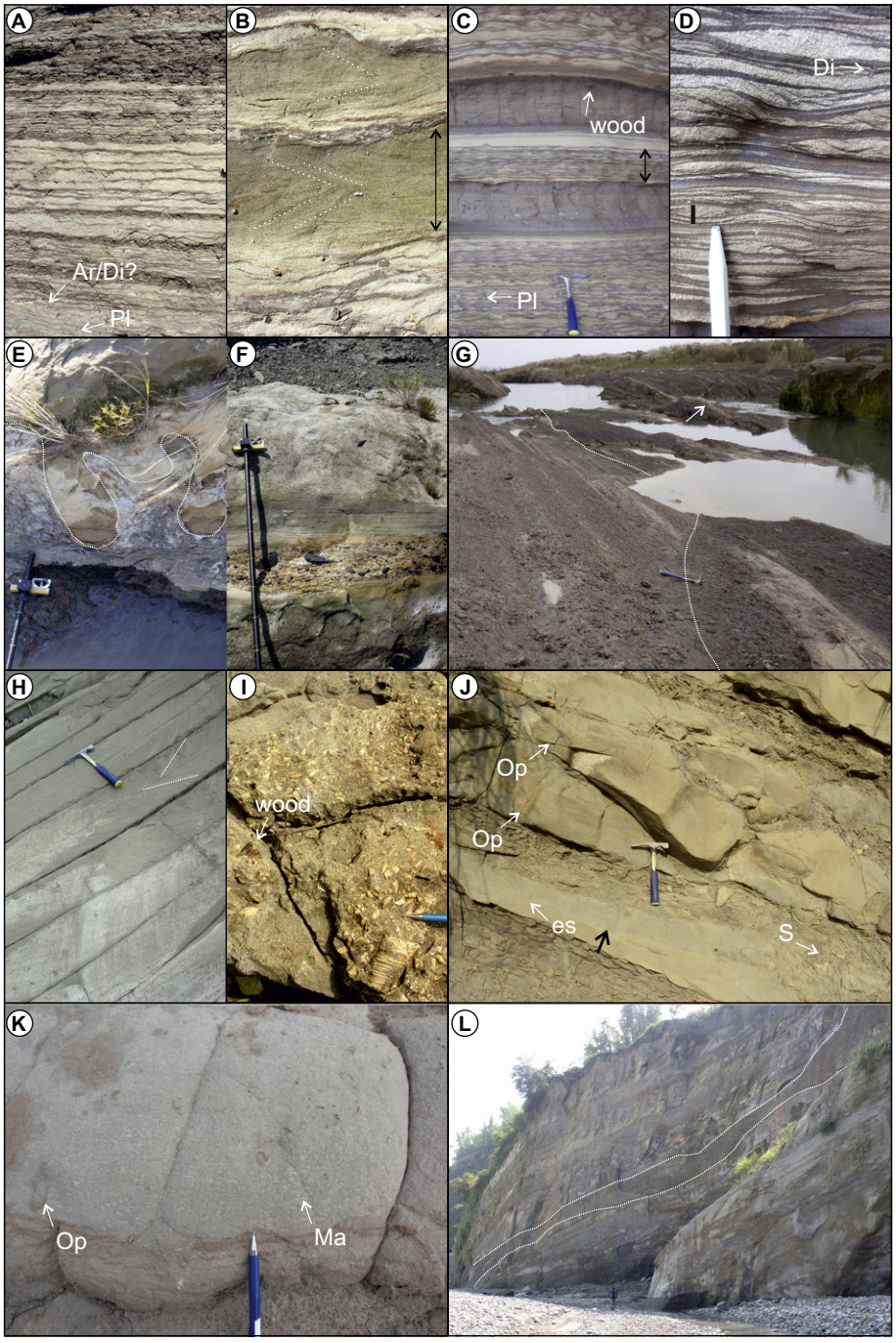

Fig. 7. (A) Mud-draped siltstone and very fine-grained sandstone beds showing vertical thinning and thickening with bidirectional current ripples; tidal flat environment, foreshore. Note the increase and decrease in sand content. Burrows are sparse to moderate and comprise traces of small suspension feeding organisms, *Diplocraterion* (Di, no horizontal cuts found), *Arenicolites* (Ar). Top Nanchuang formation, Dahan-chi section. (B) Small-scale herringbone cross beds without mud drape in between the two opposite flow directions. Arrow is five centimeters. Tidal flat environment, foreshore. Cholan formation, Dahan-chi section. (C) Close view of layer marked with black arrow is shown in (D). Thinly rhythmic lenticular- to wavy-bedded mudstone. Thick mudstone beds in between show grading from planar-laminated to structureless bedding at top. Organic matter is present, finely dispersed as well as in bigger trunks. Sand mud couplet with bidirectional current is marked with black bar in (D). Burrows are common, mainly produced by deposit and suspension feeders, *Planolites* (Pl), *Diplocraterion* (Di). Lower intertidal zone, foreshore. Nanchuang formation, Keelung. (E) Oblique view from below showing load structures of medium-grained sandstone (dashed line) on an organic-rich mudstone. Mudstone unit may contain root structures. Top view of the same unit in (F) with low angle cross bedded sandstone containing abundant organic material and mud pebbles at the base. Top of sandstone layer with climbing ripples. Storm deposition on the tidal flat, foreshore. Base Toukoshan formation, Dahan-chi section. (G) Vertical aggradation of a tidal flat. Dashed line marks the bottom of mud-dominated tidal flat with swamp/marsh deposits at the top (arrow). Nanchunag formation, Dahan-chi section. (H) Herringbone cross bedding in medium coarse, well sorted sandstone. Units are separated by thin mud layers. Fluvial dominated intertidal foreshore. Cholan formation, Tsaohu-chi section. (I) Bioclastic conglomerate associated with fluvial influenced open-marine foreshore. Conglomerates contain abundant wood fragments. Toukoshan formation, Nantou section. (J) Medium coarse sandstone with local slumping. Bioturbation was scarce evidenced by vertical structures of *Ophiomorpha* (Op) and escape burrows. Mudstone contains sea urchins (S). Black arrow points to borderline of very fine and coarse grained sandstone. Fluvial-open marine foreshore. Cholan formation, Tsaohu-chi section. (K) Parallel-laminated and cross-stratified fine-grained sand interlayered within a mudstone unit with dense *Macaronichnus* cross-cut by *Ophiomorpha*. Sub- to inter-tidal, shoreface-foreshore transition. Bottom Toukoshan formation, Pinglin-chi section, Nantou. (L) Planar-laminated and flaser-bedded, (occasionally cross-stratified) fine-grained sandstone and mudstone beds. Interlaminated thick clast-supported conglomerates with channel incision (dashed line). Toukoshan formation (Borderline Huoyenshan Member – Hsiangshan Member), Pinglin-chi section, Nantou.

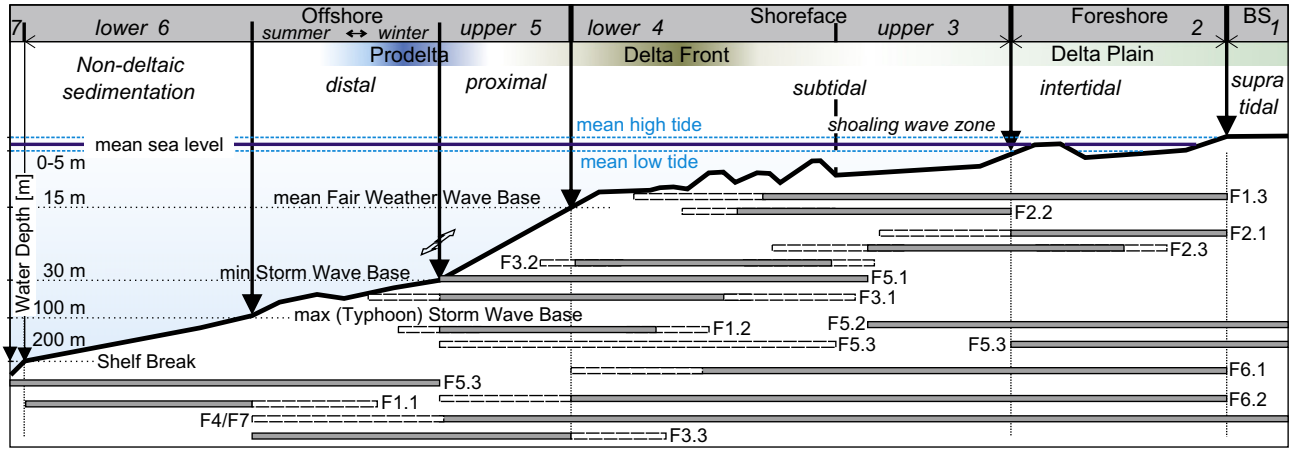

Fig. 8. Schematic depositional profile along the Taiwan orogen. The partitioning of the depositional profile follows the shoreface model of Pemberton et al. (1992), adjusted to Taiwan. The positions of the different zones are based on the position of the maximum wave base (or typhoon wave base; referring to heavy storms during the summer season from June to October), storm wave base (or minimum storm wave base during the winter from October to May), and fair-weather conditions (mean wave height and period). The distribution of the facies is shown relative to these boundaries. The facies was assigned by analyzing sedimentary structures (e.g. hummocky cross stratification), trace fossil associations and distribution, and dominating grain size.

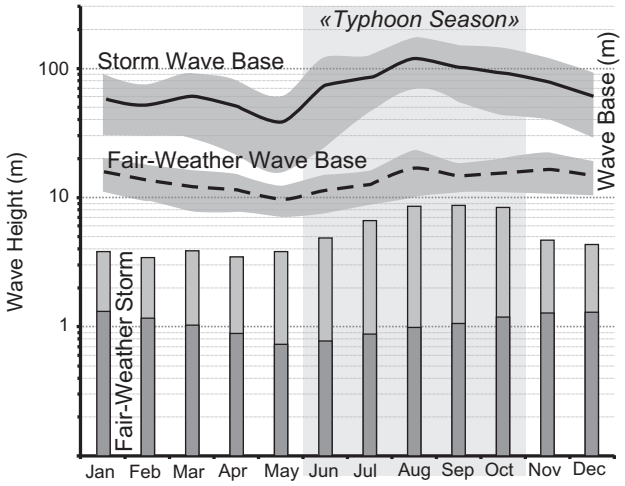

Fig. 9. Estimation of the wave base with data from the modern Taiwan Strait (Central Weather Bureau, Marine Statistics: http://www.cwb.gov.tw/eng/index.html). Fair-weather conditions are associated with mean wave height and period, storm conditions with maximum observed wave height and period, and typhoon conditions (maximum storm influence) with maximum values between the months June to October (“typhoon season”).

both with transitional boundaries. Unidirectional current ripples with small wavelength and height (<5 mm) are abundant within the silt-rich units. Unidirectional climbing ripple cross-lamination was also observed in a few sandier beds that exhibit a sharp base and transitional upper boundary into the overlying massive mudstone (Fig. 4B). The sandier beds contain also abundant finely dispersed organic matter.

Burrows are restricted normally to the top of the layers with a low diversity mixed trace fossil suite of small *Skolithos*, *Chondrites* and *Nereites*. Some facies (F1.1 and F3.2) show colonization by organisms producing small *Helminthopsis* and *Phycosiphon*.

3.3.1.1. Interpretation. The fine-grained character of these facies suggests a dominantly low-energy, suspension fallout sedimentation (Fig. 6). The sandier intervals with gradational boundaries to the top (Fig. 4B) may represent event flows, probably towards the offshore, followed by suspension fallout after high energy events such as typhoons. The absence of HCS or wave ripples in these sand beds precludes deposition above storm wave base. As typhoons lead to heavy precipitation, suspended sediment concentrations in rivers after typhoon events might have formed hyperpycnal flows as it occurs frequently today in Taiwan (Milliman and Kao, 2005). Such event flows may have reached the lower offshore and could be responsible for deposition of sandy units with unidirectional bedforms in the lower offshore.

The virtual absence of bioturbation suggests relatively high rates of deposition (perhaps linked with the frequent influx of material due to storm and/or floods in proximal environments), quiet low-oxygenated bottom water or scarcity of food. However, the subtle increase in ichnodiversity and intensity of bioturbation sometimes observed on top of sand beds suggests temporarily increased oxygenation and re-colonization with opportunistic trace producers. Bioturbated mud layers are considered to represent quiet periods of slow sedimentation (Prave et al., 1996; Savrda and Nanson, 2003). Similar facies associations deposited between mean and maximum storm wave base were described by Yu et al. (2008) in the Nantzuhsien-chi section in Southern Taiwan. These authors reported trace fossils such as *Helminthopsis*, *Zoophycos* and *Paleodictyon* commonly found in the distal *Cruziana* and *Zoophycos* ichnofacies, as well as deep-water benthic foraminifers and nannofossils. These facies are, therefore, interpreted as belonging to the lower offshore, below maximum storm wave base (e.g. typhoon wave base).

3.3.2. Upper offshore

This facies association consists of fine, mm-scale laminated lenticular bedded silty mudstones and siltstones (F1.2) irregularly interbedded with thin, fine sandstone beds (F5.1) (Fig. 4F). Sandier intervals (F5.1) show subparallel lamination and low-angle (hummocky) cross-stratification with wavelengths of ~3 to 6 m and oscillation ripples or combined flow ripple lamination on top surfaces (Fig. 4A, C, D and H). Current ripples are dominantly pointing to one direction, with few evidences of bidirectional currents. Covey (1984a) interpreted distal sand beds in the offshore assemblages as tempestites rather than turbidites based on the lack of grading, the presence of cross-stratification and the lateral thickness changes. In addition, typical features of hummocky cross stratifications such as low angle (<10–15°) bounding surfaces and laterally varying thickness of the laminations were observed (Cheel and Leckie, 1993) (Fig. 4G).

Table 1
Sedimentary facies and trace fossil occurrence in the western foreland basin of Taiwan. Lithology-code is based on (Reijers et al., 1993) (modified). Main/minor constituent, M/m mudstone, J/j siltstone, S/s sandstone, C conglomerate (ms matrix supported, bc bioclastic, cs cobbles, clast supported). p horizontal/planar lamination, w wavy/irregular lamination, l lenticular lamination, f flaser bedded, h heterolithic stratification, ma massive bedded, g graded beds/bed boundaries, x cross stratification, b bioturbated.

Facies name (Code)	Lithology and sedimentary structures	Ichnology	Interpretation	Occurrence of similar facies
Facies 1: Mud dominated units				
Planar laminated muddy siltstone and lenticular mudstone. F1.1: Mlp/MJlp/Smlp (e.g. Fig. 4B, Fig. 4E)	• Layers commonly laterally extensive with variable sand content • Thin, lenticular lenses of sand and silt • Uni- and/or (weak) bidirectional current ripples, sometimes vertically aggrading and eroding • Large scale channels (10–30 m width, 1–10 m infill height) • Low angle erosion surfaces	Bioturbation typically absent. Discrete intensely bioturbated layers may be present (tiny specimens of *Helminthopsis, Phycosiphon and Planolites), Zoophycus*	Predominantly low energy environment with rare energetic events indicated by sand laminae, possibly near typhoon storm wave base; lower offshore	• Prodelta facies associations (Carmona et al., 2009; MacEachern et al., 2005) • Distal mouth bar front deposits (Brettle et al., 2002)
Lenticular bedded mudstone and sandy siltstone. F1.2: MJl (e.g. Fig. 3D, Fig. 3E, Fig. 5D)	• Pronounced lenticular bedding • Soft-sediment deformation abundant • Low angle cross bedding • Swell-and-pinch structures • (Erosive) climbing ripple lamination • Mixed mud pebble and/or bioclastic conglomerates	Low to medium. common: *Planolites*, *Chondrites*. Rare: *Conichnus*, *Protovirgularia*, *Bergaueria*, *Tasselia*	Mixed high/low energy environment, above mean storm wave base; lower shoreface to upper offshore	• Longshore sand bars (De Raaf et al., 1977) • Distal delta front (Carmona et al., 2010) • tide dominated estuarine deposits (Hovikoski et al., 2005) • Deposits between FWB and MSW (Krassay, 1994)
Wavy to lenticular bedded mudstone and muddy siltstone. F1.3: MJw (eg., *Fig. 6A*, *Fig. 6E*, *Fig. 7A*)	• Current and/or oscillation ripples • Soft sediment deformation structures • Synaeresis cracks • "Graded" units from wavy bedded sandstones to lenticular bedded mudstones (units approx. 5–15 cm thick).	Rare traces of *Bergaueria*, *Nereites*, *Conichnus*, *Tasselia*, *Planolites*, *Siphonichnus*	Deposition near fair weather wave base, but well above the mean storm wave base; foreshore to lower shoreface	• Subtidal to lower intertidal facies (Couëffé et al., 2004) • Estuarine bay deposits (Buatois et al., 2005) • Intertidal facies (Alam, 1995) • Intertidal point bar deposits (Thomas et al., 1987) • Intertidal flat (Choi, 2004)
Facies 2: Silt and Sand dominated units				
Wavy bedded mudstone and flaser bedded sandstone. F2.1: Msw/Smw (e.g. *Fig.* 6A, Fig. 6B)	• Small scale bidirectional current ripples • Thickening-thinning of sand layers • Asymmetrical wave ripples • Low angle ripple lamination • Interference (wave) ripples on top surfaces • Dark organic material and organic clasts • Rare isolated deformation structures	Low. Small *Skolithos* and *Teichichnus*, *Thalassinoides*, *Ophiomorpha*, *Diplocraterion*, *Conichnus*	Deposition well above storm wave base, with strong currents and possible salinity stresses, strong tidal influence; the facies may be deposited on an intertidal to subtidal mixed/sand flat; foreshore to upper shoreface	• Intertidal rhythmites (Tessier, 1993) • Wave generated (tidal) sand bars (De Raaf et al., 1977) • Modern tidal flat (Collinson et al., 2006)
Massive flaser bedded sandstone interlayered with thin wavy mudstone. F2.2: Swm (e.g. *Fig.* 5J, Fig. 6J)	• (Double) mud drapes • Symmetrical wave ripples • Sand content prevailing • Amalgamated sandstone layers • Hummocky cross- and common planar cross-stratification • Small scale channels are common (width 30–50 cm, height 10–15 cm)	Low. *Thalassinoides* burrows on top surfaces, abundant *Ophiomorpha*, *Paleophycus*, *Siphonichnus*, *Planolites*, equilibrium structures, *bivalve burrows* in muddy parts cut by sandstone beds	Deposition above storm wave base; high-energy oscillatory and combined flows during repeated storm events, with stable and continuous sedimentation rates between higher energetic storm events; (upper) shoreface	• Proximal delta front deposits (MacEachern et al., 2005) • Recent subtidal sands (Walker, 2004) • Distal mouth bar front deposits (Brettle et al., 2002)
Planar laminated flaser bedded sandstones. F2.3: Sf *(e.g. Fig.* 5H, Fig. 6K)	• flaser bedding • interference (wave) ripples on top surfaces • symmetrical and asymmetrical wave ripples	Low to absent. Few *Ophiomorpha*	Deposition during tractive bottom currents and subsequent waning high energy events locally reworked by waves; stressful physicochemical conditions due to shifting substrate; upper shoreface to foreshore	• Lowest occurrence of Ophiomorpha nodosa in the beach and near beach areas below mean low tide (Frey et al., 1978) • Distal mouth bar front deposits (Brettle et al., 2002)

(*continued on next page*)

Table 1 (*continued*)

Facies name (Code)	Lithology and sedimentary structures	Ichnology	Interpretation	Occurrence of similar facies
Facies 3: Bioturbated units				
Bioturbated, massive muddy siltstone and silty mudstone. F3.1: Jmb (e.g. *Fig. 3G*)	• Low to abundant fossil debris and mollusks • Massive-appearing • Scarce medium coarse sandstones • Planar cross-stratification	Variable, but generally completely bioturbated. Common: *Teichichnus*. *Thalassinoides*, *Ophiomorpha*, *Siphonichnus*, *Diplocraterion*, *Schaubcylindrichnus*, *Asterosoma*, *Planolites*, *Paleophycus*, *Sea urchins*	Deposition in a low energy area primarily from suspension, above mean storm wave base; protected, (probably) brackish water environment; rare energetic events are indicated by disseminated sand and shell debris; lower shoreface to offshore	• Schaubcylindrichnus formosus is interpreted as a filter feeding worm living in offshore sand bar and shoreface environments (Löwemark and Hong, 2006)
Bioturbated, massive, siltstone and sandstone. F3.2: Jsb (e.g. *Fig. 5F*, *Fig. 5G*)	• Massive-appearing silt- and sandstone • Thin lenses of mud pebble conglomerate • Two different units: • (1) A sandy siltstone with low diversity, but locally medium to high bioturbation with Schaubcylindrichnus of different sizes or Ophiomorpha burrows and mud pebble conglomerates • (2) a muddy sandstone with high bioturbation and diversity	Medium to high. *Schaubcylindrichnus*. The size varies from a few mm to 10–15 cm length and 0.2–1 cm width. *Ophiomorpha*, *Phycosiphon*, *Planolites*, *Cylindrichnus*, *Teichichnus*, *Chondrites*, *Paleophycus*, *Polykamton eseri/Hilichnus*, few sea urchins	Deposition in a low energy environment with sporadic higher sand influx, possibly due to hyperpycnal flows and turbidity conditions and/or bottom currents; lower shoreface	• Polykampton eseri was recognized in a deep marine, offshore environment (Wetzel and Uchmann, 1998) • Schaubcylindrichnus formosus is interpreted as a filter feeding worm living in offshore sand bar and shoreface environments (Löwemark and Hong, 2006)
Completely bioturbated muddy siltstone and sandstone. F3.3: MSwb (e.g. *Fig. 3C*, *Fig. 6L*)	• Massive-appearing mud with interspersed organic material • Wavy to lenticular bedding still evident • Rare unburrowed mud pebble conglomerates • Shell-debris sporadically distributed throughout the deposit	High with abundant equilibrium and escape traces; *Planolites*, *Siphonichnus*, *Paleophycus*, *Schaubcylindrichnus*, *Skolithos*, *Sea urchins*, *Teichichnus*, *Thalassinoides*, *Phycosiphon*, *Rosselia*, *Bivalve*	Low energy open marine depositional environment, sporadically influenced by storm deposits; lower shoreface to upper offshore	• Storm dominated distal delta front, lower to upper offshore (Buatois et al., 2008)
Facies 4: Cross laminated units				
Crossbedded sandstone and siltstone. F4: Sx/Jx (e.g. Fig. 3F, Fig. 4B, Fig. 4C, Fig. 4D, *Fig. 4G*)	• Trough cross stratified fine to medium grained sandstone (Sxt) • Low angle, planar cross bedded very fine to medium coarse sandstone (Sxp) • Hummocky- and Swaley cross-stratification in fine to medium coarse sandstones (Sxu) • Herringbone cross-stratification in medium to coarse grained sandstones (Sxv) • Climbing ripple cross laminated, very fine to fine sandstones. (Sxrcl)	Low to absent. Rare. Rare *Ophiomorpha*, *Paleophycus*. Scarce *Skolithos*. Absent	Deposition of high energy wave-induced currents and (subordinate) tidal currents; backshore to lower offshore (Typhoon wave base)	
Facies 5: Massive/interlayered units				
Parallel to subparallel layered massive sandstone and sandy siltstone. F5.1: SJpx (e.g. Fig.5H, 5I)	• Deformation/erosion structures • Unidirectional current ripples, small scale bidirectional current ripples, interference ripples; (single) mud drapes • Low angle cross-stratification • Small scale channels, lateral thinning of sandstone layers (20–30 m)	Low. Abundant escape structures, *Planolites*, *Thalassinoides*, *Conichnus*, *Paleophycus*. rare: *Taenidium*	High-energy oscillatory and combined flows during storms, deposition below fair-weather wave base, but well above storm wave base; upper offshore to upper shoreface	• Proximal to distal delta front deposits (MacEachern et al., 2005) • Offshore sand bars (Frey et al., 1978)

Table 1 (*continued*)

Facies name (Code)	Lithology and sedimentary structures	Ichnology	Interpretation	Occurrence of similar facies
Well sorted, laminated sandstone. F5.2: Sp (e.g. *Fig. 7E*, *Fig.* 7H, Fig. 7J, Fig. 7K)	• Small scale planar cross-stratification; herringbone cross-stratification • Abundant load structures, horizontal planar lamination • Bioclastic conglomerates	Low. *Ophiomorpha*, *Skolithos*, *Maccaronichnus*, rare escape structures	High energy deposition in a proximal source area, common with fluvial deposits in a marine environment; upper shoreface, foreshore to backshore	• (Meandering) River deposits (Gani and Alam, 2004) • Floodplain/Sheet flood deposits (Hjellbakk, 1997)
Massive mudstone. F5.3: Mma (e.g. *Fig.* 4A, Fig. 4B, Fig. 4E, Fig. 7G)	• Massive, structureless beds with min. 10 cm thickness • Faint graded beds very rare • Very thin silt laminae (less than 1 mm) • Laterally extensive	Rare-no bioturbation observed. Rare *Ophiomorpha* and *Skolithos* burrows on the top/base surfaces	Low-energy, suspension fallout in the absence of waves and currents; slack water conditions in nearshore to backshore; floodplain deposition	• Swamp/marsh deposits (Rahmani, 1988)
Facies 6: Heterolithic stratified units				
Rhythmically layered mudstone and sandstone. F6.1: SMh (e.g. *Fig.* 5A, Fig. 5E, Fig. 6F)	• Flame and load structures • Double mud drapes • Symmetrical wave ripples • Interference ripples • Abundant organic material, finely dispersed • Planar cross-stratification • Small scale scours (dm)	Moderate to high. *Large Macaronichnus* (Savrda and Uddin, 2005), *Paleophycus*, *Scolicia*, *Ophiomorpha*, *Planolites*, *Cylindrichnus*, *Siphonichnus*	Deposition during alternating high/low energy conditions with mud deposition during slack water periods within intertidal to subtidal environment; (lower) shoreface to foreshore	• High energy tidal inlet sequence (Savrda and Uddin, 2005) • Tidal sand bars in a high energy shoreface environment (Aguirre et al., 2010) • Maccaronichnus: high-energy tidal channel and upper shoreface/foreshore settings (MacEachern and Pemberton, 1992) • Lower intertidal zone, China (Fan et al., 2004)
Wavy and planar laminated muddy siltstone and sandstone. F6.2: SJh (e.g. *Fig.* 5J, Fig. 5K)	• Fine laminated (mm), heterolithic stratification • Unimodal, small scale current ripples (<0.5 mm), scarce/faint bimodal current ripples, climbing ripples • Synaeresis cracks • Deformation structures • Low angle channel structures (10–15 m width, 1–1.5 m height)	Low to medium. *Planolites*, *Paleophycus*, *Taenidium*, *Protovirgularia*, *Nereites missouriensis*, *Gyrochorte*, *Conichnus*, *Helminthopsis*, *Lockeia*, *Gordia*	Stressed environment with alternating low/high energy conditions in an intertidal to subtidal environment. Upper offshore to foreshore	• Tidally influenced sand-rich mouthbar (Brettle et al., 2002) • Estuarine tidal channels and intertidal point bar deposits (Choi, 2010) • Macrotidal estuarine valley (Buatois et al., 1997) • The trace fossil Protovirgularia has been found in distal delta front settings (Carmona et al., 2010) • Prodelta subtidal rhythmites (Miller and Eriksson, 1997)
Facies 7: Conglomerate units				
Conglomerates. F7: Ccs/Cms/Cbc (e.g. Fig. 3F, Fig. 7F, *Fig.* 7I, Fig. 7L)	• Clast-supported conglomerate • Mud pebble conglomerate • Bioclastic conglomerate	No to rare bioturbation. The grain size of the sediment is a controlling factor on the occurrence and type of bioturbation (Dashtgard et al., 2008)	Backshore to offshore	• Braided river channel deposits (Miall, 1978, 1996) (Similar deposits can be studied in rivers draining the Taiwan mountains today. These rivers are characterized by high discharge variability and near mountain source)

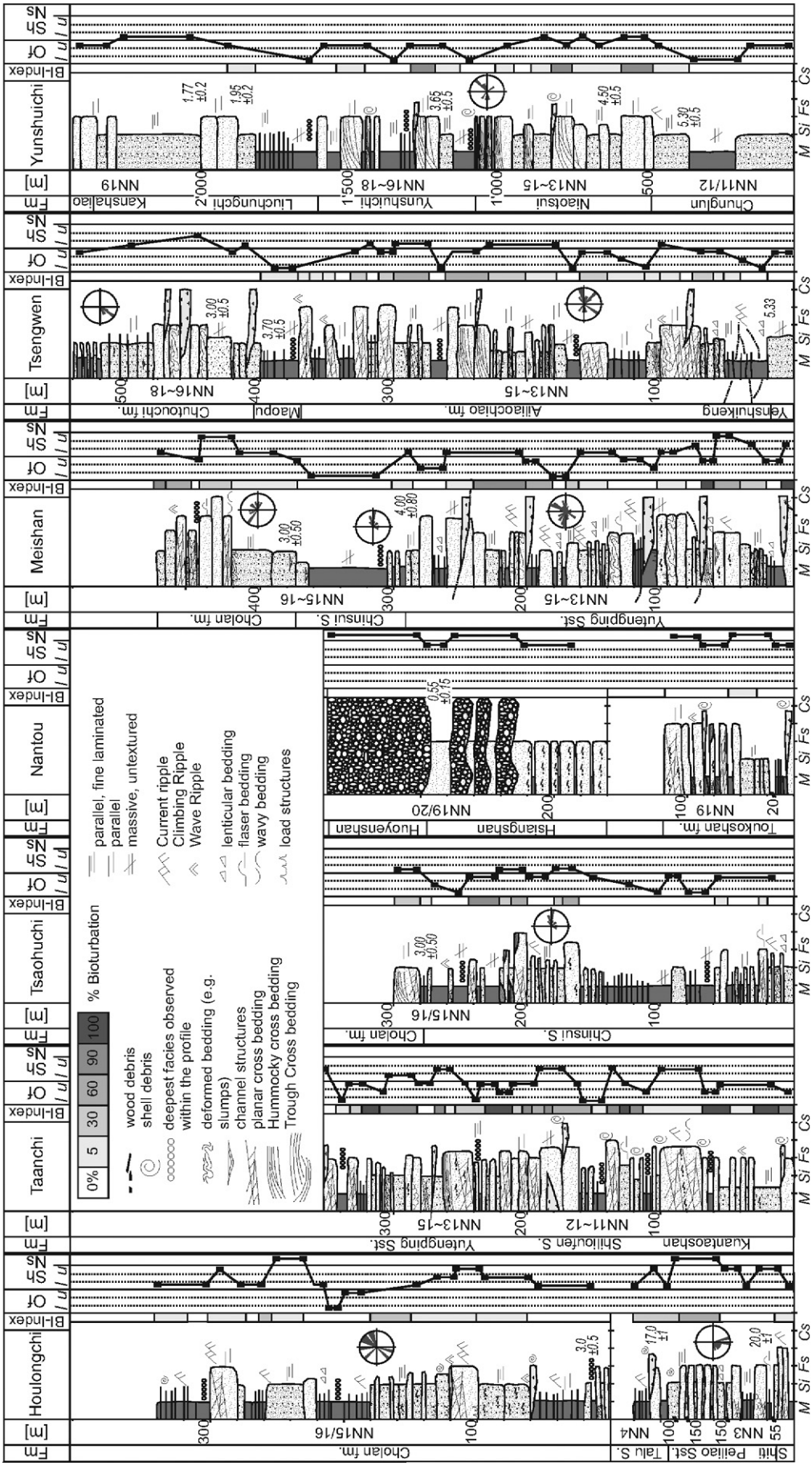

Fig. 10. Representative vertical stratigraphic sections used for interpretation and correlation of data published in literature; vertical lithological logs, sedimentary structures and bioturbation index (Taylor and Goldring, 1993). Flow direction of current ripples and cross-stratification is plotted as rose diagrams. The formation affiliation is based on the geological maps and lithologic characteristics within the given stratigraphic range. The ages and NN-zonation are based on literature (see text for explanation). Of = Offshore, Sh = Shoreface, Ns = Nearshore (foreshore-backshore), M = Mud, Si = Silt, Fs = fine sand, Cs = Coarse sand.

The sandstone beds may be amalgamated into 2–10 m thick sandstone packages separated by cm-thick mudstone layers or mud pebble conglomerates (F4/F5.1/F7) (Fig. 3D, F and D and G). The upper parts of the amalgamated sandstone bodies (F4) contain bioclastic mud pebble conglomerates (F7) and small shell fragments. The conglomerates have a matrix very similar to the surrounding sandstones beds and are composed of rip-up clasts of fine laminated sandy mudstone probably derived from the underlying units. Some finely dispersed organic material (wood and leaf fragments) is present within the sandy parts (F4/F5.1/F7). Sparse small scale erosional features forming channel-like structures 10's of cm to several dm in width cut into underlying mudstone facies (F1.2/F5.3) (Fig. 3A and B). Locally, soft-sediment deformation structures occur (F5.1) (Fig. 4D). Mud dominated units (F1.2/F5.3) contain weak, sometimes rhythmic occurrences of silty layers.

Bioturbation is commonly extensive and obliterates original lamination in the mudstones (F1.2/F3.3) (Fig. 3G). Sandstone intervals show variable degree of bioturbation ranging from complete homogenization (F3.1) to very low to absent bioturbation within the sharp based erosive beds (F5.1). The sandstone beds show low diversity and low abundance with *Skolithos*, *Ophiomorpha*, *Planolites* and escape traces. The bulk suite of identified traces consists of *Teichichnus*, *Planolites*, *Phycosiphon*, *Palaeophycus*, *Schaubcylindrichnus*, *Chondrites*, *Tasselia*, *Conichnus* and *Bergaueria*. Small-sized *Zoophycos* isp. having 5–15 cm wide lobes were found in muddy sandstone units of F3.3 in the Chutouchi formation in the Tsengwen-chi section (Zu-Malai-Farm).

3.3.2.1. Interpretation. The alternation between fine to medium sandstones and mudstones, the presence of oscillation and/or combined flow ripples on top of hummocky cross stratified fine sandstones suggests the alternation of storm events within a generally calm background sedimentation, thus below fair-weather wave base but above storm wave base.

The trace fossil assemblages are typical of the distal *Cruziana* ichnofacies and to a minor extent of the *Skolithos* ichnofacies that is restricted to the colonized storm beds, in combination indicative of upper offshore conditions (Pemberton et al., 1992). The occurrence of *Zoophycos* in this shallow marine setting is unusual but was, for instance, also described from the North Alpine foreland basin in Austria (Pervesler and Uchmann, 2004).

The seasonal variation in storm frequency, intensity and circulation in the Taiwan Strait produces a comparable variation in wave size and period (Wang, 2004) and therefore, the wave base. This hydrodynamic pattern not only influences the sediment distribution along the coastline but also perpendicular to it due to the shifting wave base (see Section 3.2). The seasonal sedimentation pattern in the Taiwan foreland basin is best preserved in the distal upper offshore (e.g. prodelta deposits, Fig. 4E), and proximal upper offshore (e.g. delta front deposits, Fig. 3E).

Whereas the lower offshore displays no HCS bedding, the distal upper offshore contains discrete sandstone beds with well-preserved hummocky-cross stratification within a mud-dominated succession. HCS beds in the distal parts show distinctly well-pronounced wave ripples (Fig. 4H) and abundant current ripples. More proximal, the individual HCS beds grade into thick, sometimes amalgamated, fine laminated m-thick sandstone units with planar cross- and hummocky cross-stratification. Thin lag deposits, small gutter casts and erosional scours appear together with an increase in trace fossil diversity. The trace fossil assemblage in the proximal upper offshore resembles graded storm sand beds observed from offshore Indonesia (Pemberton et al., 2001).

3.3.3. Lower shoreface

The lower shoreface deposits consist of fine to medium grained, planar laminated, wavy to flaser bedded 10's of cm to m thick sandstone (F2.3) intercalated on a millimeter- to cm-scale with wavy to lenticular (F1.2) and rhythmic bedded mudstone and muddy siltstone units (F6.2) (Fig. 5D). Soft-sediment deformation and synaeresis cracks are locally abundant within the wavy bedded mudstones (F1.3). Interlaminated massive sandstone units (F4) show commonly planar and hummocky cross-stratification and may be amalgamated to thick sandstone units of several meters separated by erosional surfaces (Fig. 5J and K). Rhythmically bedded fine to medium grained sandstones with mm-to-cm thick mudstone–siltstone interlaminations (F5.1) occur above sandstone units (F4) or below wavy bedded mudstone facies (F1.3). Lamination and bedding surfaces are subparallel, and beds appear massive and laterally persistent across exposures with a thickness of several tens of meters. Sandstones (F2.3/F4/F5.1) show combined flow ripple lamination and oscillation ripples (Fig. 5H and I). Mud pebbles are distributed within the sandier beds and conglomerates (F2.3/F4/F5.1/F7). Organic material occurs more frequently than in the offshore deposits. Accumulations of complete and broken shells occur as small scoured lags at the base of sandstones (F3.1/F4) and small scale scours with a width between cm to dm or as laterally extensive layers of several cm's.

Bioturbation within the heterolithic layers (F6.2) is low and indicates mainly deposit feeding structures of *Nereites*, *Protovirgularia*, *Planolites*, *Helminthopsis*, *Cylindrichnus*, *Lockeia*, *Arenicolites*, *Diplocraterion* and *Gordia* (Fig. 5B/5C). Muddy sandstones (F3.2) show *Schaubcylindrichnus*, *Ophiomorpha* and *Planolites*. The degree of bioturbation is highly variable and trace fossil assemblages mainly match the *Cruziana* ichnofacies, while *Skolithos* ichnofacies is restricted to sandier event beds with escape traces and equilibrium traces (Fig. 6F). *Palaeophycus* is the most striking trace fossil found in the shoreface assemblages.

3.3.3.1. Interpretation. Persistent wave action is indicated by the presence of symmetrical and asymmetrical oscillation ripples resultant from combined flows, and by flaser bedded sandstone beds. Waves and storms not only reworked the sediment, but were also highly efficient in separating mud and sand (Fig. 5A). This process forms amalgamated sand layers with low to absent mud partings in between. Similar sand bodies have been described on a high energy coast of Australia, where large waves and bottom currents force seaward sand movement in water depths of up to 80 m (Field and Roy, 1983). The lower shoreface deposits thus consist of sandy mud and muddy silt and progressively grade into fine to medium sandstones in the upper shoreface (Fig. 6H and I). This finding is supported by recent studies of sediment distribution in the modern Tsengwen-chi delta (Hong et al., 2004).

The bidirectional ripple cross-stratification and presence of mud drapes documents variations of flow velocity and direction which is typical of settings with strong tidal influence (Fig. 6J) (Willis et al., 1999). Additionally, common rip-up mud clasts suggest tidal influence (Dalrymple and Choi, 2007). Fair-weather deposits consist of dark grey massive, sandy siltstone and muddy sandstone (F3.1, F3.2) (Figs. 5F and 6L); they are extensively bioturbated and thoroughly homogenized.

3.3.4. Upper shoreface

This facies association is composed of m-thick, well-sorted, planar stratified siltstone and very fine to fine sandstone (F5.1) with abundant organic fragments, shell debris and rip-up mud clasts. Planar cross- and trough cross-stratification occur on mm- to m-scales and are often characterized by discontinuous mud drapes on the foresets (Fig. 6K). Massive medium to coarse sandstone beds (F2.1/F2.2/F4/5.1) may be present exhibiting fine lamination and low to high angle cross-stratification (Fig. 6G). The sandstone beds are sharp based and usually thin and thicken over lateral distances of 10–20 m (F4). Lenticular to wavy bedded mudstones (F2.1) are

interlayered with cm- to 10's of cm-thick, massive and flaser bedded sandstones (F2.3) showing combined flow ripple lamination and interference ripples on top surfaces (Fig. 5I). Wavy and lenticular bedded cm-scale heterolithics of mud-dominated siltstones (F6.1) show mm to cm high asymmetric ripples often with weak bidirectional flow azimuths and climbing ripple lamination (Fig. 6C and D). Massive laterally continuous sandstones show flaser and subordinate wavy bedding that usually occur transitionally above wavy to lenticular bedded mudstones (F2.2). Deformation structures in mud-rich parts (F2.1/F5.1/F7) and slumping up to several m in size are abundant (Fig. 5H). Lag deposits of broken fossils and mudclasts are locally present.

Trace fossils occur in low diversity and low abundance (F3.2), but escape and equilibrium burrows are frequent (Fig. 6F and I). The common trace fossils are ascribed to the proximal *Skolithos* ichnofacies and consist of *Skolithos*, *Ophiomorpha*, *Planolites*, *Conichnus* (Fig. 6B) and *Schaubcylindrichnus*. Large *Macaronichnus*-like traces (Savrda and Uddin, 2005), *Scolicia*, *Phycosiphon*, *Chondrites* and rare *Teichichnus* may be observed additionally.

3.3.4.1. Interpretation. The grain size, near absence of mudstone partings within the sand dominated units (F2.1/F2.2/F2.3/F4/F5.1) and abundant high-angle cross-stratification support deposition within a high energy environment. These findings are supported by predominantly vertical and deep penetrating trace fossil assemblage forming part of the *Skolithos* ichnofacies.

The dominance of wave energy overprints tidal influence, but it is nonetheless evident from rhythmic sand-mud couplets (F6.1). Protected bay margin systems can show such thin bedded rhythmic, lenticular and flaser bedded, mud-dominated facies with variable tidal influence (F1.3/F2.2/F6.1). The low diversity and commonly low density trace fossil assemblage is consistent with the shallow brackish water setting representing a stressed ecosystem (Beynon and Pemberton, 1992).

3.3.5. Foreshore

Under foreshore here, two distinct facies associations are summarized. The first facies association consists of brownish, rhythmic mm-to-cm-scale bedded wavy and lenticular mudstone (F6.1) interlaminated with up to 10 cm thick sandstone (F2.3). Sharp based medium grained sandstone layers (F2.1) are irregularly interlaminated and show symmetrical ripples on top surfaces (Fig. 6A). Bidirectional current ripples, oscillation ripples and (rhythmic) climbing ripples are frequent. Erosive, m-thick sandstone beds show fine planar lamination and low to high angle cross beds (F5.2), separated by mm-to-cm-thick wavy bedded mudstone layers (F1.3). Abundant channel systems occur and are composed of medium coarse, planar laminated, usually dark grey-greenish sandstones of several dm thickness with low angle cross-stratification (F5.2) interlaminated with massive wavy bedded mudstones (mm-dm) (F1.3). The sandstones show mm- to cm-thick flaser bedding, oscillation ripples and flame structures (F2.1). Bioclastic conglomerates and mud pebble conglomerates (F7) occur at the base of the sandstones (F5.2, F4).

Organic material occurs dispersed as fine debris within the beds, but also whole trunks with up to 50 cm in diameter and dm-thick layers showing weathering in rusty-yellow patches (Fig. 7F). Shell debris is common on the basal surface of the sandstones (F4), but occurs also chaotically distributed in the massive mudstones (F3.1/F5.3). On top of these follow dm to m thick layers of dark massive mudstones (F5.3) with abundant organic material such as well preserved leaves, plant debris, root casts and ostracodes (Fig. 7G).

Burrows are locally abundant comprising size-reduced forms in low diversity (Fig. 7C and D). Trace fossils are restricted to suspension feeding organisms with vertically, to some extent also horizontally penetrating domiciles of *Skolithos* ichnofacies (*Skolithos*, *Ophiomorpha*, *Palaeophycus*, *Planolites*, *Teichichnus*).

The second facies association comprises very fine to coarse, well sorted sandstones (F5.2), in parts with well rounded cm-sized gravels and rare horizontally aligned mud pebbles (Fig. 7J). Planar lamination and high-angle cross bedding is common. The sandstone layers may be separated by thin wavy to lenticular bedded, mm- to several cm-thick mud layers (F1.3). Syndepositional deformation structures, small scale climbing ripple lamination, double mud draped bidirectional flow ripples and bioclastic conglomerates are common (Fig. 7I). Organic material occurs in mm- to cm-thick layers. Burrows are sparse to absent with rare *Skolithos* and *Ophiomorpha*, escape traces and remains of sea urchins and crabs. *Macaronichnus segregatis* (Savrda and Uddin, 2005) occur in up to 30 cm thick sandstones (F2.1).

3.3.5.1. Interpretation. The foreshore environment records deposition between mean low and mean high tide (e.g. Reading and Collinson, 1996). The structures observed in the first facies association strongly indicate alternating flows with inclined heterolithic stratification (successive sand/mud couplets) and rhythmic climbing ripple cross lamination. Similar characteristics were reported from intertidal deposits of the Amazonian foreland basin (Hovikoski et al., 2008), the Korean Bay (Choi, 2010) or the Mont-Saint-Michel Bay in France (Tessier, 1993) and include root and rhizome structures, flaser-, wavy- and lenticular-bedding, (tidal) channels and deformation structures. This is interpreted here as being indicative of the intertidal zone.

The dominance of medium to coarse-grained sandstones containing well rounded gravel and layers of bioclastic conglomerates with well preserved shells and oysters suggest fluvial deposition. Because of their association with bidirectional current ripples, double mud draped flow ripples and few trace fossils of the *Skolithos* ichnofacies as well as the increased appearance of herringbone cross stratification, these deposits are interpreted as fluvial dominated intertidal sediments.

3.3.6. Backshore

These facies consists of poorly sorted granule to boulder grade clasts (maximum clast size 1 m) in a medium to coarse sandy matrix. Clasts are angular and/or platy to well-rounded. Vague imbrication is apparent in some beds, but more commonly clasts are randomly oriented. Poorly to well sorted very fine to very coarse sandstone layers with a maximum thickness of approximately 20 m are intercalated within bioclastic conglomerates. The sandstones are commonly channelized and laterally extensive (Fig. 7L). The sandstone layers may also show low to high angle cross bedding and isolated pebbles on the basal layer (F4). Burrows are very rare and restricted to the *Skolithos* ichnofacies and escape structures. The mud-dominated intervals may contain abundant residue of crabs.

Interpretation: The coarse grain size with clasts and pebbles of up to 1 m indicates that these facies were deposited by strong currents. The interlayered sandstone beds associated with the conglomerates are interpreted as fast deposition during reduced flow conditions because of the abundance of (steep) climbing ripple lamination and cross stratification. The degree of sorting, clast shape and facies architecture resembles fluvial sediments that were deposited in the Coastal Plain by modern rivers draining the Taiwan mountain range.

Covey (1984a) described two fluvial facies within the foreland basin; a sandy fluvial lithofacies assemblage resembling meandering river deposition, and a cobbly braided river lithofacies assemblage, which is comparable to modern cobbly braided river

Table 2
Data from well logs and stratigraphic sections consulted for interpretation to construct the paleogeographic maps. Interpretation of depositional environment effectively used for the paleogeographic maps are in italic. Numbers in brackets are interpolated/arguable, mainly subsurface data from well logs or where biostratigraphic age is doubtful. Numbers refer to the depositional profile (Fig. 8).

	Age (Ma)				
Well/Section	12.5 ± 1.0	5.5 ± 0.5	3.0 ± 0.5	2.0 ± 0.2	0.5 ± 0.15
BJP-1	*(4)*[25]	*6*[25]/(4/5)[18]	*(3)*[25]	*(3)*[25]	*(1.5)*[25]
CC-1	*(5)*[25]	*(5)*[25]	3/4[14]/*5.5*[25]	3/4[14]/*5.5*[25]	3/4[14]/*5.5*[25]
Chiayi	–	–	3/4[14,25]	3/4[14,25]	2/3[14,25]
Chinanshan	*(5)*[25]	*(5.5)*[25]	3/4[14]/*4*[25]	3/4[14]/*3.5*[25]	1[14]
Chunkungliao/Nantou	2/3[6,25]	3/4[6]/*3.5*[25]	3/4[6,14,25]	3/4[6,14,25]/*4.5*[25]	*1*[6,14,25]
CLI-1	*(5)*[25]	*(6)*[25]	3/4[14]/*5.5*[25]	3/4[14]/*5*[25]	5/6[14]/*5.5*[25]
CS-53	3/4[6,7]/*3.5*[25]	*3*[6,25]	*(2.5)*[25]	*(2.5)*[25]	*(1.5)*[25]
CT-1	3/4[6,7]/*3.5*[25]	*3*[6,25]	*(2.5)*[25]	*(2.5)*[25]	*(2)*[25]
Dahanchi	*1.5*[25]/2/3[24,25]	*3*[25]/*4*[24,25]	3/4[24]/*3.5*[25]	*2.5*[25]/3[24,25]	*2*[24,25]
HK-4	*(3)* [25]	*(2.5)* [25]	*(2.5)* [25]	*(2.5)*[25]	1/*2*[2]
HL-2	*3*[25]/4[14]	*(3.5)* [25]	*3*[25]/4[14]	3/4[14]/*3.5*[25]	*1*[14]
HM-3	*(5)* [25]	*(5.5)* [25]	*(5)* [25]	3/4[14]/*5*[25]	*2.5*[25]/3/4[14]
Hukouchi	–	*(3/4)* [12]	*(3/4)* [25]	*(3/4)* [25]	*(1/2)*[2,12]
Houlong	3/*4*[8,9,25]	*3*[25]/4[8,9]	*3*[25]/4[8,14]	3/4[14]/*3.5*[25]	1/3[11,14]/*1.5*[25]
HP-1	*(6)* [25]	*(5.5)* [25]	3/4[14]/*5*[25]	5/*6*[14,25]	*2.5*[25]/3/4[14]
Huoyenshan	*4.5*[25]	*3.5*[25]	*3*[25]	3/4[14]/*3.5*[25]	*1*[14,25]
Keelung	*2/3B*	*2/3B*	*(3/4)* [25]	*(2.5)* [25]	*(2)* [25]
KT-1	*3*[25]/4[6,7]	*(2.5)*[6,25]	*(3)* [25]	*(3)* [25]	*(3)* [25]
Kuanmiao	5/6[14]/*6.5*[25]	3/4[14]/*4.5*[25]	5/6[14]/*5.5*[25]	*4.5*[25]/5/6[14]	1/*2*[2,14]/*1.5*[25]
Kueichungchi	*(4.5)* [25]	*(3.5)* [25]	*(3)* [25]	*3*[16,25]	*3.5*[16,25]
KY-1	3/4[6,7]	*(3)*[6,25]	*(2.5)*[25]	*(2.5)*[25]	1/*2*[2,25]
Linkou	*(5)*[25]	*(3)*[25]	*(3.5)*[25]	1[14]/*1.5*[25]	*1*[14,25,A]
Liuchungchi	5/6[3]/*5.5*[25]	3/*4*[3,25]	*3.5*[25]	*3*[25]/4/6[3,20]	1/*2*[20]/*2.5*[25]
Liushuangkeng	*(4.5)*[25]	*(4)*[25]	*(3.5)*[25]	*(3)*[25]	1/*2*[16,20]/*3*[25]
LK-1	*(5)*[25]	(4/5)[18]/*(4)*[25]	*(4)*[25]	*(4)*[25]	*(1.5)*[25]
LT-1	*(6)*[25]	*(5)*[25]	*5.5*[16,25]	*5*[25]/6[14,16]	3/*4*[14,16,25]
Meishan	*(3)*[25]	(3/4[23])/*4*[25]	3/4[23]/*3.5*[25]	*3*[25]/3/4[23]	*2*[25]
MH-1	*(6)*[25]	*(6)*[25]	*(5.5)*[25]	*(4.5)*[25]	(1/*2*[2])/*1.5*[25]
Mucha	*5*[25]/6[13]	*6*[25]/6[12,13]	*5.5*[25]/6[12,13]	*3.5*[25]/6[12,13]	*2*[25]/4/6[13]
Nantzuhsien	5/*6*[17,22,25]	*4*[25]/5/6[17,22]	*4.5*[25]/5/*6*[17,22]	*(3)*[25]	*(2)*[25]
Neiping	*4*[6,25]	*3*[6,25]	*(2.5)*[25]	*(3)*[25]	*(1.5)*[25]
PC-1	*3*[25]/4[14]	*3.5*[25]	*3*[25]/4[14,16]	*2.5*[25]/5/6[14,16]	*1.5*[25]/5/6[14,16]
PCC-1	*(6)*[25]	*(4)*[25]	5/*6*[14,25]	3/4[14]/*5*[25]	(1/*2*[2])/*1.5*[25]
PH-1	*(2/3)*[25]	3/4[18,19]/*3.5*[25]	*5*[25]/6[18,19]	*6*[18,19]	6/*7*[18,19]
Pinglinchi	*(4)*[25]	*(3)*[25]	*(2.5)*[25]	*(4)*[25]	1/*2*[10]/*1.5*[25]
PK-3	*(3)*[25]	*(3.5)*[25]	3/*4*[14,25]	*3*[25]/4[14]	3/4[14]/*3.5*[25]/(1/*2*[2])
PKS-1	*(5)*[25]	*(5.5)*[25]	5/*6*[14,25]	3/*4*[14,25]	*2*[14,25]
PPS-2	3/4[14]/*4.5*[25]	*(6)*[25]	2[14]/*5*[25]	*5*[25]/6[14]	5/6[14]/*5.5*[25]
PS-3	3/4[7]/*3.5*[25]	*(3)*[25]	*(2.5)*[25]	*(2.5)*[25]	2/*3*[2]/*2.5*[25]
PTG-1	*(5)*[25]	3/*4*[14,25]	*(3.5)*[25]	2[14]/*2.5*[25]	*1*[14]
Shihmen	3/*4*[7,25]	*3*[25]/4[7]	*(2.5)*[25]	*(2)* [25]	*(1.5)*[25]
Taan River	*(3*[25]*)*	*3.5*[25]	*3*[25]	*3*[25]	*(2)*[25]
TAC-1	–	–	3/4[14]/*3.5*[25]	3/4[14]/*3.5*[25]	*3*[25]/4[14]
Takeng	*(5)*[25]/(6)[18]	3/*4*[18,25]	*3.5*[25]/3/4[18]	*(2.5)*[25]	*(1)*[25]/*2*[2,14]
TC-1	*(6)*[25]	*(5)*[25]	5/*6*[14,25]	*5.5*[25]/5/6[14]	*2*[14]
TCS-2	3/4[6,7]/*3.5*[25]	*3*[6,25]	*(3)*[25]	*(3)*[25]	(1/*2*[2])/ *1.5*[25]
TCS-8	3/4[7]/*3.5*[25]	*(3)*[25]	*(3)*[25]	*(3)*[25]	(1/*2*[2])/ *1.5*[25]
TEL-1	2[19]/*2.5*[25]	3/4[19]/*3.5*[25]	3/*4*[19,25]	*5*[25]/6[19]	*5*/6[19]
THS-5	*(3)*[25]	*(3)*[25]	3/4[14]/*5*[25]	3/*4*[14,25]	3/4[14]/*3.5*[25]
TN-1	*(6)*[25]	*(5.5)*[25]	5/*6*[14,25]	5/*6*[14,25]	3/4[14]/*5*[25]
Touchienchi	*(5)*[25]/6	*(4)*[25]	3/4[20]/*3.5*[25]	3/*4*[20,25]/5/*6*[19]	*3*[20,25]/5/*6*[19]
TS-1	–	–	–	*(1/2)*[2]	1/*2*[2]/*1.5*[25]
Tsaohuchi	*3*[25]/4[6]	3/*4*[6,25]	4/5[21]/*4.5*[25]	*3*[25]/4[21]	*1.5*[25]
Tsengwen	*(6)*[25]	*4*[25]/5/6[1,4]	*3.5*[25]/3/4[1,4,21]	*3*[25]/4[2,8,21]	*2.5*[25]/3/4[21]
WG-1	*(3)*[25]	*(3)*[25]	2[14]/*2.5*[25]	3/*4*[14,25]	3/4[14]/*3.5*[25]
Wuchi	*3.5*[25]/4[15]	*(3.5)*[25]/(3/4[15])	*(3)*[25]	*(2.5)*[25]	*(1.5)*[25]
YC-1	5/*(6)*[25]	*(6)*[25]	*(5)*[16,25]	*(5)*[16,25]	1/*2*[2]/*3*[16,25]
Yunshuichi	5/*6*[3,5,25]	2[3.5]/*3*[19,25]	3/*4*[17,19,25]	3/4[3,5,19]/*3.5*[25]	1/*2*[2,10]/*2.5*[25]

[1]Huang (1967), [2]Lee (1963), [3]Chiu (1968) and Wu (1970), [4]Chou (1968), [5]Wu (1968), [6]Chou (1970, 1971), [7]Chang (1971), [8]Hu and Yang (1975), [9]Huang (1976a,b), [10]Chou (1977), [11]Hu (1977), [12]Huang (1977), [13]Chow (1980), [14]Covey (1984a), [15]Chiu (1972), Huang (1986), [16]Chang (1968), Chang and Chi (1983), Liew (1988), [17]Ting et al. (1991), [18]Yeh and Chang (1991), [19]Yeh and Yang (1994), [20]Hong (1997), [21]Chen et al. (2001), [22]Yu et al. (2008), [23]Castelltort et al. (2011), [24]Pan (2011), and [25]this study.

lithofacies (Miall, 1996). For simplicity, the massive conglomerate deposits of the Toukoshan fm. and associated fluvial lithofacies (appearing at the top of Cholan fm.) were attributed to the backshore environment. In the modern Coastal Plain, fluvial deposition occurs between elevations of 0 to a few tens of meter. Therefore, the backshore is defined here as the entire area following above the foreshore.

4. Paleogeographic evolution

4.1. Methodology

4.1.1. Age model

Biostratigraphic data from well logs and stratigraphic sections are used to constrain key reference time horizons (Berggren

Table 3
Maximum amount of shortening (30% error estimate) in km and % of length of the cross-section. Results are based on eight balanced cross-sections across the Western foreland basin (Mouthereau and Lacombe, 2006; Mouthereau et al., 2001).

Nearby sections	Shortening (max.) (km)	Shortening (%)
1/Chuhuangkeng	13 (17)	20
2/Taan-chi	8 (10.4)	8
3/Tsaohu-chi	11 (14.3)	25
4/Meilin	22 (28.6)	36
5/Meishan	20 (26)	35
6/Yushing	8 (10.4)	13.5
7/Kuanmiao	24 (33.6)	21.5
8/Alien	11 (14.3)	14.3

et al., 1995). The calcareous nannofossil-zones are the best studied and have been used to date the foreland deposits in previous investigations, and also offer the best spatial coverage of the basin. Detailed sedimentologically logged sections in combination with biostratigraphic data were used to characterize stratigraphic sections of the Western Foothills. Important synthesis of Neogene calcareous nannofossil biostratigraphy has been made by several authors (Chang and Chi, 1983; Chou, 1973; Huang and Huang, 1984), among others. Within the publicly available database for Taiwan, the nannofossil zone boundaries that are best documented are NN19/NN20 (middle to late Pleistocene: 0.5 ± 0.15 Ma), NN18/NN19 (early Pleistocene: 2.0 ± 0.2 Ma), NN15/NN16 (late Pliocene: 3.5 ± 0.5 Ma), NN11/NN12 (late Miocene to early Pliocene: 5.5 ± 0.5 Ma) and NN5/NN6 (middle Miocene: 12.5 ± 1.0 Ma). These ages were used as key reference time horizons.

4.1.2. Construction of the facies-grid

Each depositional environment was given a number between 1 (backshore) to 7 (slope to bathyal). This code forms the basis to describe the prevailing depositional environment at each time horizon for each of the sections described in this work (Fig. 10), as well as for the sections published in literature and for well logs. Table 2 summarizes the interpreted data of the published sections and well logs.

When it was not interpreted by the authors, a depositional environment was assigned to the data based on the author's description. Main criteria include grain size, sedimentary structures, stratigraphic position and published previous map relationships. Geographic location and environment code were then entered into a GIS database and the environmental trends were interpolated between the data points using linear interpolation. The final domains shown on the map are intentionally restricted to the area close to the data points because interpolation to the map boundaries may lead to irrelevant artifacts.

4.1.3. Restoration of pre-shortening position

The sections and wells located within the Western Foothills (Fig. 1) have been displaced westward due to the collision-induced thrusting. Deformation may have initiated as early as 5 Ma, but most or all is Pliocene and younger (Mouthereau and Lacombe, 2006; Mouthereau et al., 2001). The total shortening recorded in eight balanced cross-sections perpendicular to the orogen (parallel to the direction of transport) were used to restore the positions of the facies data points (Table 3), to their position at the NN11/NN12 boundary (5.5 ± 0.5 Ma). Between NN11/NN12 and the modern, position was linearly interpolated to estimate location at intermediate intervals NN19/NN20 (0.5 ± 0.15 Ma), NN18/NN19 (2.0 ± 0.2 Ma) and NN15/NN16 (3.5 ± 0.5 Ma). It is assumed that the position of these data at the NN5/NN6 boundary was the same as at the NN11/NN12 boundary because both are prior to collision.

4.2. Results and discussion

The resulting maps (Fig. 11) represent snapshots of the sedimentary landscape at key instants of the history of the basin of Taiwan.

4.2.1. Middle Miocene (12.5 Ma) to early Pleistocene (2 Ma)

The physiography of the basin seems to change very little from the middle Miocene (Fig. 11A) to the early Pleistocene (Fig. 11D) with a distribution of facies that is essentially maintained from the passive margin to the foreland stage. Particularly evident is an isolated shoal that is well known as the Peikang High (Meng, 1967). It probably represents a horst inherited from the extensional phase and stratigraphic data indicates that it remained a topographic high through the middle to late Pleistocene. Also, the paleo-shelf break located in the south remained in a position very close to its modern location from 12.5 to 3.5 Ma.

The proximal–distal facies trend in the middle Miocene is essentially directed to the South–East, with an axis roughly parallel to the current Asian passive margin. This is especially visible in the northern half of the map area. The Northern and Western parts were covered by shallow marine shoreface and foreshore sediments associated with the Asian margin (Fig. 11A). This situation subsequently evolved, as in the early and late Pliocene (Figs 11B and C) the basin deepens both to the North and to the South. In the early Pleistocene, the proximal–distal trend in the north is reversed with a single trend to deeper water towards the South-West.

The second important observation is the widening and slight deepening of the basin at 3.5 Ma (Fig. 11C). This is the time of deposition of the mud-dominated Chinshui shale, interpreted by Covey (1984a) as the "underfilled" stage of the foreland basin. This clearly marks accelerating subsidence presumably caused by the approach of the growing orogen. Interestingly, even though the facies change at this time is prominent, the depositional water depth remained shallow, because these sections are situated high on the continental margin, so that we do not observe deeper water facies. We suggest that increasing subsidence led to the westward retreat of facies belts at the Asian margin and hence, coarse material was trapped further to the west. The growing Taiwan orogen, however, was only capable to deliver fine-grained material to the basin as indicated by slate fragments and reworked nannofossils from the Central Range (Chang and Chi, 1983; Huang, 1967; Lee, 1963).

In the early Pleistocene (Fig. 11D), while the Peikang High and surrounding basins are still present and represent the preceding physiography, the general bathymetric trend changed in response to loading by the approaching orogen. The axis of maximum water depth moved westward and the eastern side of the basin was uplifted and became eroded. In addition, the previously bathyal southern part of the basin became filled with distal shelf and slope sediments.

4.2.2. Early Pleistocene (2 Ma) to present

From 2 Ma to the present configuration, significant changes have occurred due to the approach of the orogen. The proximal parts of the basin have evolved into a wedge-top setting introducing deformation and sedimentation (DeCelles and Giles, 1996). Simultaneously along the entire length of the orogen terrestrial deposition with fluvial facies and deposition of deep marine facies migrated from the central and northern parts to the south-west (Fig. 11E). Today, maximum water depth coincides with the central axis of the Taiwan Strait (Fig. 11F). The various shoaling areas within the strait are related to inherited topographic highs, which represent modern equivalents of the former Peikang High. The considerable water depth of modern Taiwan Strait is very likely a consequence of the interglacial sea-level highstand.

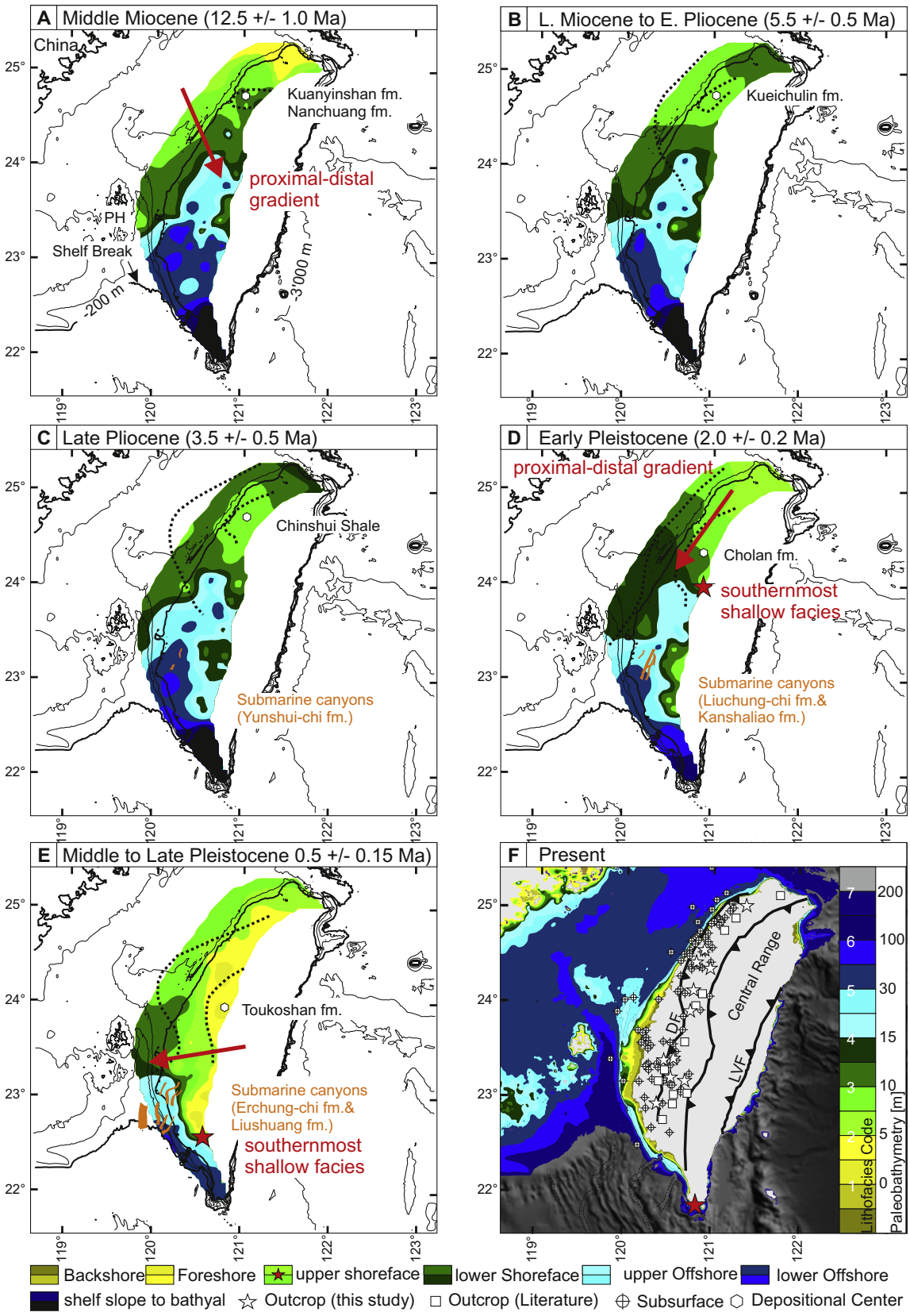

Fig. 11. Paleogeographic maps for the Taiwan foreland basin. Biostratigraphic (calcareous nannofossils) and sedimentological data are used for each map (for details see text). The maps illustrate the development of facies in front of the west- and southward migrating orogen. Red star indicates the maximum extent of the upper shoreface, measured from the northern tip of Taiwan along strike the longitudinal valley (N°20). White hexagons show the main depot centers of the specific formation delineated from isopach maps with maximum and zero isolines (Shaw, 1996; Simoes and Avouac, 2006). Indicated in orange are submarine canyon systems observed on seismic profiles (Fuh et al., 2003). The outline of present-day Taiwan and the modern bathymetry are indicated for reference.

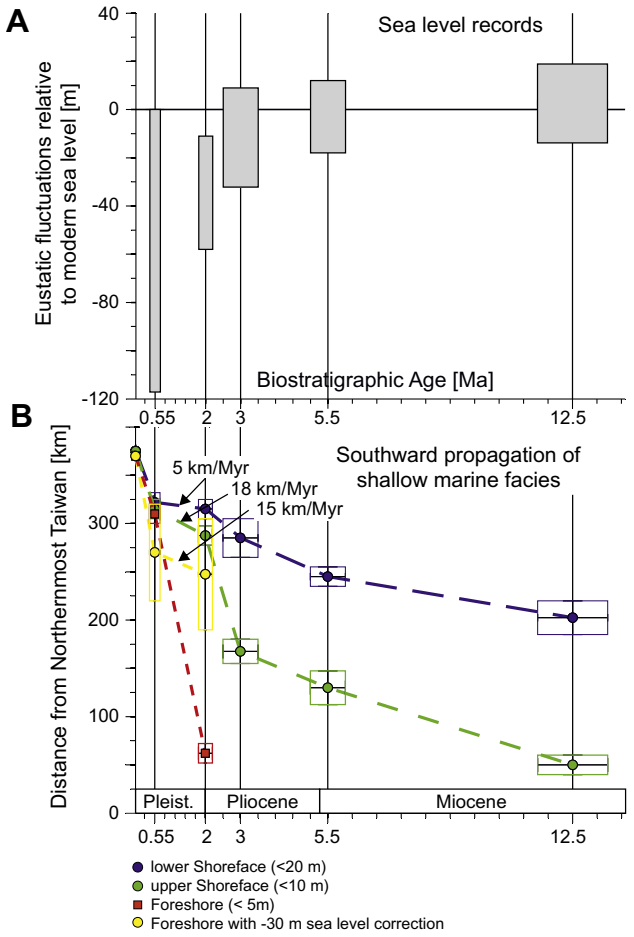

Fig. 12. Southward displacement of shallow marine facies during oblique arc-continent collision. (A) Water depth estimates from middle Miocene to late Pleistocene with error box according to the biostratigraphic ages (e.g. first and last appearance) used in this study (Miller et al., 2011). (B) Influence of the proximal orogen is evident from late Pliocene. Mean southward propagation rates increase considerably from 0.5 Ma to the present (106–120 km/Myr). The shallowest facies (e.g. foreshore) is strongly influenced by sea-level fluctuations during the late Pleistocene when glacial eustatic amplitudes are highest. The influence of sea-level change on facies propagation was estimated by assuming a mean sea level 30 m lower than modern. The data points for the paleogeographic maps are based on the depositional profile (see Fig. 8).

4.2.3. Paleogeographical changes versus depocenter migration

The southward migration of shallow marine facies (e.g. upper shoreface) is mainly visible during the last stage of foreland evolution between early and late Pleistocene (Fig. 11D and E). Between 2 Ma and 0.5 Ma, average southward propagation rates are low and range between 5 km/Myr and 20 km/Myr, except for the foreshore (165 km/Myr) which is considerably higher due to the influence of sea level variations (Fig. 12A). From 0.5 Ma to 0 Ma, southward migration accelerated considerably (106–120 km/Myr) (Fig. 12B). The sediment depocenter in the northern part of Taiwan migrated at rates between 26 and 41 km/Myr (Simoes and Avouac, 2006), which is slightly faster than the southward evolution of shallow marine facies in front of the growing orogen. This demonstrates the complicated basin-wide pattern of sediment distribution and accumulation in the evolving foreland basin. By 2 Ma the main sediment depocenter has migrated southwards considerably, contemporaneous with the change of proximal – distal facies boundary. The migration of the sediment depocenter to the Southwest also led to an increased longitudinal sediment transport out of the basin. This is reflected in the development of approximately NE–SW oriented submarine canyons located in the main basinal axis, which is parallel to the active mountain front.

5. Discussion: orogen-basin evolution

The Western Taiwan foreland basin represents a classical peripheral foreland basin system (DeCelles, 2012). Its basin fill is affected by the oblique collision between the Luzon volcanic arc and the Asian passive margin. In Taiwan, deep marine offshore deposits in the Western Foothills are restricted to a narrow NE–SW trending basin. They lack characteristic turbidite successions commonly found in the early stages of foreland basins, due to the limited flexural response of the Asian continental crust to the Taiwan orogenic load. This lack of overdeepening lead to persistent shallow marine, mainly shoreface deposits throughout the history of the Taiwan foredeep. Any synorogenic deep marine turbidites (related to the early stages of basin evolution) deposited further to the East of our study area were likely uplifted and eroded away as the collision propagated towards the south.

Currently south of Taiwan the accretionary wedge is colliding with the South China slope (Yu and Huang, 2009). There, the accretionary wedge is comprised of west vergent thrust faults and characteristic features of wedge-top depocenters (Chiang et al., 2004; Yu and Huang, 2006). The transition from accretionary wedge to foreland basin is hardly preserved in the stratigraphic record as coeval basins are most likely uplifted and eroded away during the process. Studies of this transition in the North Alpine foreland basin show that inherited rift margin structures exerted a major control on the foredeep formation (Gupta and Allen, 2000; Lihou and Allen, 1996). Earlier findings related to a tectonic context suggested that the Taiwan orogen eventually reached a steady size (Suppe, 1981), implying steady loading and sediment fluxes into the basin. However, even in this stage, the load continued to migrate to the west.

The longitudinal redistribution of sediments as observed in the western foreland basin of Taiwan can be compared with sediment transport routes in other well known foreland basins. The North Alpine Molasse basin, for example, shows two cycles of fluvial dominated environments (Lower and Upper Freshwater Molasse) interrupted by a shallow marine cycle (Upper Marine Molasse, Allen et al., 1991). The high energy environment of the shallow marine system may have provided a similar mechanism for sediment (re-)distribution as today in the Taiwan Strait (Covey, 1984a; Homewood and Allen, 1981). Sediment transport and dispersal within the modern Taiwan Strait is complex and strongly controlled by seasonal changes (Jan et al., 2002; Wu et al., 2007), with the highest discharge during typhoon-induced floods in the summer months (Milliman et al., 2007; Xu et al., 2009). These sediments are reworked and transported north- and southwards out of the Taiwan Strait into the South China Sea and Okinawa Trough/East China Sea (Kao et al., 2008; Liu et al., 2008).

As sedimentation rates increased, the basin filled to sea level and continental sedimentation dominated. The sediment was redistributed along strike, in the proximal parts by large alluvial fans and in the distal parts by fluvial systems. Another example is the foreland basin in front of the Southern Pyrenees (Puigdefàbregas et al., 1992). Here, active thrust-faults and contemporaneous uplift formed numerous isolated intramontane basins, which then progressively filled to form large continental to lacustrine basins during the Eocene to Oligocene. They also exhibit longitudinal sediment transport out of the basin, during periods of basin connection with the marine system.

An initial geodynamic setting similar to Taiwan but having a different basin history is encountered in the Solomon Sea near Papua New Guinea (Galewsky and Silver, 1997). The oblique collision

between the Bismarck forearc and the Australian margin formed a foredeep which filled very rapidly. The basin fill records a long period of deep marine turbiditic deposition (1.5–3.0 Ma) and a very short phase of shallow marine to fluvial conditions (ca. 100 kyr). The difference arises from the physiographical differences between the Australian and Asian continental margins. The narrow and steep Australian continental margin creates a closed system which affects sedimentation rates and dispersal patterns preventing a steady-state in the foredeep. While in Taiwan, the broad comparatively flat Asian continental margin allowed shallow marine conditions to persist throughout the entire history of the basin development (this study, Covey, 1984a). Here, the preserved steady-state foredeep deposits consist of prograding shallow marine to fluvial deposits as the orogen migrates onto the Asian margin (Covey, 1986). Even though modern erosion rates and sediment fluxes are high (Dadson et al., 2003) and probably are highest since the initial collision in Pliocene times, the basin is not overfilled or filled to sea level as it opens to the south.

The high energy environment of the Taiwan Strait (similar to the Upper Marine Molasse stage in the Alps) may be the controlling mechanism to balance the sediment budget by efficient longitudinal transport to the deep water South China Sea (Allen et al., 1991; Covey, 1986). This is further supported by the fact that the modern and ancient shelf of Southwest Taiwan is incised by several submarine canyons (see also Fig. 11, Fuh et al., 2003). These submarine canyons are likely conduits for sediment on the shelf to be transported out of the foreland basin (Yu and Hong, 2006).

6. Conclusion

The progressively changing sedimentary system of the Taiwanese foreland basin is governed by the oblique collision between the Luzon volcanic arc with the Asian continental margin. Sedimentological investigations provide new insights into the collision history and growth of the Taiwan orogen. The main findings are:

(1) Based on a system of sixteen main lithofacies, grouped into seven facies associations we found that shallow marine environments persisted for most of the basin development.
(2) Typhoons may have been underestimated in their importance on generating substantial resuspension of the sediment across most of the Taiwan shelf. The succession of HCS beds in the stratigraphic column, which can be linked to the influence of typhoon-generated waves, may be the result of a seasonal signal.
(3) From middle Miocene (12.5 Ma) to early Pleistocene (2 Ma), the paleogeographic changes are small. The distribution of facies is maintained from the passive margin with a proximal–distal facies trend towards the South–East and a basin axis parallel to the Asian passive margin.
(4) The basin subsidence increased during the late Pliocene (3.5 ± 0.5 Ma), and the basin started to become wider and deeper.
(5) Since the early Pleistocene (from 2 Ma) to the present the proximal–distal facies trend is clearly reversed to the southwest. The basin today is dominated by the large sediment flux from the orogen in the East.
(6) The distribution of facies belts within the basin strata forms a basis for calculating rates of southward propagation. We obtain 5–20 km/Myr from 2 Ma to 0.5 Ma, and 106–120 km/Myr between 0.5 and 0 Ma. The late Pleistocene rates of facies belt migration are considerably higher possibly due to the influence of sea level variations during glacial-interglacial cycles.
(7) The paleogeographic maps document the southward migration of facies belts driven by large sediment fluxes out of the orogen. We suggest that there is an important export of sediment longitudinally to deep water depocenters which is sufficient to prevent the basin from becoming overfilled or even fully terrestrial with marine facies persisting throughout the foreland basin stage.

Acknowledgements

We would like to thank two anonymous reviewers for constructive reviews which improved the manuscript. Many thanks to Shao-Ping Chiang, Chinen-Nan "Mr. Paul" Yang, Tsun-You "Heavy Metal" Pan, Shih-Lin Tesng and Pei-Hua Hsu for their assistance in the field, as well as the whole Basin Research Group from NCU. We also thank Jack, Olimpia and Maja Giletycz for their help and welcome. This project was funded by SNSF Swiss National Science Foundation Grant Number #200020-131890.

References

Aguirre, J., de Gibert, J.M., Puga-Bernabéu, A., 2010. Proximal–distal ichnofabric changes in a siliciclastic shelf, Early Pliocene, Guadalquivir Basin, southwest Spain. Paleogeography, Paleoclimatology, Paleoecology 291, 328–337.
Alam, M.M., 1995. Tide-Dominated Sedimentation in the Upper Tertiary Succession of the Sitapahar Anticline, Bangladesh, Tidal Signatures in Modern and Ancient Sediments. Blackwell Publishing Ltd., pp. 329–341.
Allen, P.A., Crampton, S.L., Sinclair, H.D., 1991. The inception and early evolution of the North Alpine Foreland Basin, Switzerland. Basin Research 3, 143–163.
Barrier, E., Angelier, J., 1986. Active collision in Eastern Taiwan: The Coastal Range. Tectonophysics 125, 39–72.
Beaumont, C., 1981. Foreland basins. Geophysical Journal of the Royal Astronomical Society 65, 291–329.
Berggren, W.A., Kent, D.V., Swisher, C.C., Aubry, M.P., 1995. A revised Cenozoic geochronology and chronostratigraphy. In: Berggren, W.A., Kent, D.V., Aubry, M.P., Hardenbol, J. (Eds.), Geochronology, Time Scales and Global Stratigraphic Correlations. SEPM Special Publications, pp. 129–212.
Beynon, B.M., Pemberton, S.G., 1992. Ichnological signature of a bracksih water deposit: an example from the lower Cretaceous Grand Rapids formation, Cold Lake Oil Sands area, Alberta. In: Pemberton, S.G. (Ed.), Applications of Ichnology to Petroleum Exploration. SEPM Core Workshop No. 17, Calgary.
Booth, J.S., Winters, W.J., 1991. Wave Processes and Geologic Responses on the Floor of the Yellow Sea, From Shoreline to Abyss. SEPM (Society for Sedimentary Geology), pp. 123–132.
Brettle, M.J., McIlroy, D., Elliott, T., Davies, S.J., Waters, C.N., 2002. Identifying cryptic tidal influences within deltaic successions: an example from the Marsdenian (Namurian) interval of the Pennine Basin, UK. Journal of the Geological Society, London 159, 379–391.
Buatois, L.A., Mángano, M.G., Maples, C.G., Lanier, W.P., 1997. The paradox of nonmarine ichnofaunas in tidal rhythmites: integrating sedimentologic and ichnologic data from the late Carboniferous of Eastern Kansas, USA. Palaios 12, 467–481.
Buatois, L.A., Gingras, M., MacEachern, J.A., Mángano, M.G., Zonneveld, J.-P., Pemberton, S.G., Netto, R.G., Martin, A., 2005. Colonization of brackish-water systems through time: evidence from the trace-fossil record. Palaios 20, 321–347.
Buatois, L.A., Santiago, N., Parra, K., Steel, R., 2008. Animal–substrate interactions in an Early Miocene wave-dominated tropical delta: delineating environmental stresses and depositional dynamics (Tácata Field, Eastern Venezuela). Journal of Sedimentary Research 78, 458–479.
Burbank, D.W., Beck, R.A., Raynolds, R.G.H., Hobbs, R., Tahirkheli, R.A.K., 1988. Thrusting and gravel progradation in foreland basins: a test of post-thrusting gravel dispersal. Geology 16, 1143–1146.
Burbank, D.W., PuigdefÀBregas, C.A.I., MuÑOz, J.A., 1992. The chronology of the Eocene tectonic and stratigraphic development of the eastern Pyrenean foreland basin, northeast Spain. Geological Society of America Bulletin 104, 1101–1120.
Carmona, N.B., Buatois, L.A., Ponce, J.J., Màngano, M.G., 2009. Ichnology and sedimentology of a tide-influenced delta, Lower Miocene Chenque Formation, Patagonia, Argentina: trace-fossil distribution and response to environmental stresses. Paleogeography, Paleoclimatology, Paleoecology 273, 75–86.
Carmona, N.B., MÁNgano, M.G., Buatois, L.A., Ponce, J.J., 2010. Taphonomy and paleoecology of the bivalve trace fossil protovirgularia in deltaic heterolithic facies of the Miocene Chenque formation, Patagonia, Argentina. Journal of Paleontology 84, 730–738.

Castelltort, S., Nagel, S., Mouthereau, F., Lin, A.T.-S., Wetzel, A., Kaus, B.D.W.S., Chiang, S.-P., Chiu, W.-Y., 2011. Sedimentology of early Pliocene sandstones in the south-western Taiwan foreland: Implications for basin physiography in the early stages of collision. Journal of Asian Earth Sciences 40, 52–71.

Chang, S.S.L., 1968. Regional stratigraphic study of neogene formations in Chiayi-Hsinying area, West-Central Taiwan, China. AAPG Bulletin 52, 2438–2465.

Chang, S.S.L., 1971. Regional stratigraphy and petroleum possibilities of Miocene formations in Northwestern Taiwan, China. AAPG Bulletin 55, 1838–1865.

Chang, S.S.L., Chi, W.-R., 1983. Neogene nannoplankton biostratigraphy in Taiwan and the tectonic implications. Petroleum Geology of Taiwan 19, 93–147.

Cheel, R.J., Leckie, D.A., 1993. Hummocky cross-stratification. In: Wright, V.P. (Ed.), Sedimentology Review, vol. 1. Blackwell Scientific Publications.

Chemenda, A.I., Yang, R.-K., Stephan, J.F., Konstantinovskaya, E.A., Ivanov, G.M., 2001. New results from physical modelling of arc-continent collision in Taiwan: evolutionary model. Tectonophysics 333, 159–178.

Chen, Y.-G., Liu, T.-K., 1996. Sea level changes in the last several thousand years, Penghu Islands, Taiwan strait. Quaternary Research 45, 254–262.

Chen, W.-S., Ridgway, K.D., Horng, C.-S., Chen, Y.-G., Shea, K.-S., Yeh, M.-G., 2001. Stratigraphic architecture, magnetostratigraphy and incised-valley systems of the Pliocene–Pleistocene collisional marine foreland basin Taiwan. Geological Society of America Bulletin 113, 1249–1271.

Chen, H.-W., Lee, T.-Y., Wu, L.-C., 2010. High-resolution sequence stratigraphic analysis of Late Quaternary deposits of the Changhua Coastal Plain in the frontal arc-continent collision belt of Central Taiwan. Journal of Asian Earth Sciences 39, 192–213.

Chi, W.-R., 1978. The late neogene nannobiostratigraphy in the Tainan foothills region, Southern Taiwan. Petroleum Geology of Taiwan 15, 89–125.

Chi, W.-R., Huang, H.M., 1981. Nannobiostratigraphy and paleoenvironments of the late Neogene sediments and tectonic implications in the Miaoli area, Taiwan. Petroleum Geology of Taiwan 18, 111–143.

Chiang, C.-S., Yu, H.-S., Chou, Y.-W., 2004. Characteristics of the wedge-top depozone of the southern Taiwan foreland basin system. Basin Research 16, 65–78.

Chiu, H.T., 1968. Geologic structure of the Hsitaopang area, Miaoli, NW Taiwan. Petroleum Geology of Taiwan 6, 33–43.

Chiu, H.T., 1972. Miocene stratigraphy of the Nantou area, Central Taiwan. Petroleum Geology of Taiwan 10, 159–177.

Chiu, H.T., 1975. Miocene stratigraphy and its relation to the palaeogene rocks in west-central Taiwan. Petroleum Geology of Taiwan 12, 51–80.

Choi, K.S.D.R.W., 2004. Recurring tide-dominated sedimentation in Kyonggi Bay (west coast of Korea): similarity of tidal deposits in late Pleistocene and Holocene sequences. Marine Geology 212, 81–96.

Choi, K., 2010. Rhythmic climbing-ripple cross-lamination in inclined heterolithic stratification (IHS) of a macrotidal estuarine channel, Gomso bay, west coast of Korea. Journal of Sedimentary Research 80, 550–561.

Chou, J.-T., 1968. A stratigraphic and sedimentary analysis of the Protoquarzite in the Miocene Talu Shale in northern Taiwan. Petroleum Geology of Taiwan 6, 115–138.

Chou, J.-T., 1970. A stratigraphic and sedimentary analysis of the miocene in Northern Taiwan. Petroleum Geology of Taiwan 7, 145–189.

Chou, J.T., 1971. A sedimentologic and paleogeographic study of the neogene formations in the Taichung region, Western Taiwan. Petroleum Geology of Taiwan 9, 43–66.

Chou, J.-T., 1972. A sedimentologic and paleogeographic study of the upper cenozoic clastic sequences in the Chiayi region, Western Taiwan. Petroleum Geology of Taiwan 10, 141–158.

Chou, J.-T., 1973. Sedimentology and paleogeography of the upper Cenozoic system of Western Taiwan. Proceedings of the Geological Society of China 16, 111–143.

Chou, J.T., 1977. Sedimentology and Paleogeography of the Pleistocene Toukoshan formation in Western Taiwan. Petroleum Geology of Taiwan 14, 25–36.

Chou, J.-T., 1980. Stratigraphy and sedimentology of the Miocene in Western Taiwan. Petroleum Geology of Taiwan 17, 33–52.

Chow, J., 1980. Late Neogene paleoenvironments of the Mucha section in Kaohsiung. Petroleum Geology of Taiwan 17, 89–98.

Chung, C.T., 1968. Regional stratigraphic and structural study of the Tainan Foothills area, Southern Taiwan. Petroleum Geology of Taiwan 6, 15–31.

Collinson, J.D., Thompson, D., Mountney, N., 2006. Sedimentary Structures, third ed. Terra Publishing Harpenden, Herts, England.

Couëffé, R., Tessier, B., Gigot, P., Beaudoin, B., 2004. Tidal rhythmites as possible indicators of very rapid subsidence in a foreland basin: an example from the Miocene marine Molasse formation of the Digne foreland basin, SE France. Journal of Sedimentary Research 74, 746–759.

Covey, M., 1984a. Sedimentary and Tectonic Evolution of the Western Taiwan Foredeep. Unpublished Ph.D. Thesis.

Covey, M., 1984b. Lithofacies analysis and basin reconstruction, Plio-Pleistocene Western Taiwan Foredeep. Petroleum Geology of Taiwan 20, 53–83.

Covey, M., 1986. The Evolution of Foreland Basins to Steady State: Evidence from the Western Taiwan Foreland Basin, Foreland Basins. Blackwell Publishing Ltd., pp. 77–90.

Dadson, S.J., Hovius, N., Chen, H., Dade, W.B., Hsieh, M.L., Willett, S.D., Hu, J.C., Horng, M.J., Chen, M.C., Stark, C.P., Lague, D., Lin, J.C., 2003. Links between erosion, runoff variability and seismicity in the Taiwan Orogen. Nature (London) 426, 648–651.

Dalrymple, R.W., Choi, K., 2007. Morphologic and facies trends through the fluvial–marine transition in tide-dominated depositional systems: a schematic framework for environmental and sequence-stratigraphic interpretation. Earth-Science Reviews 81, 135–174.

De Raaf, J.F.M., Boersma, J.R., Gelder, A.v., 1977. Wave-generated structures and sequences from a shallow marine succession, lower Carboniferous, County Cork, Ireland. Sedimentology 24, 451–483.

DeCelles, P.G., 2012. Foreland Basin Systems Revisited: Variations in Response to Tectonic Settings, Tectonics of Sedimentary Basins. John Wiley & Sons, Ltd., pp. 405–426.

DeCelles, P.G., Giles, K.A., 1996. Foreland basin systems. Basin Research 8, 105–123.

Dorsey, R.J., Lundberg, N., 1988. Lithofacies analysis and basin reconstruction of the Plio-Pleistocene collisional basin, Coastal Range of Eastern Taiwan. Acta Geologica Taiwanica 26, 57–132.

Dashtgard, S.E., Gingras, M.K., Pemberton, S.G., 2008. Grain-size controls on the occurrence of bioturbation. Paleogeography, Paleoclimatology, Paleoecology 257, 224–243.

Fan, D., Li, C., Wang, P., 2004. Influences of storm erosion and deposition on rhythmites of the upper Wenchang formation (upper Ordovician) around Tonglu, Zhejiang province, China. Journal of Sedimentary Research 74, 527–536.

Field, M.E., Roy, P.S., 1983. Offshore transport and sand-body formation: evidence from a steep, high-energy shoreface, southeastern Australia. Journal of Sedimentary Petrology 54, 1292–1302.

Frey, R.W., Howard, J.D., Pryor, W.A., 1978. Ophiomorpha: its morphologic, taxonomic, and environmental significance. Paleogeography, Paleoclimatology, Paleoecology 23, 199–229.

Fuh, S.-C., Liu, C.-S., Wu, M.-S., 1997. Migration of canyon systems from Pliocene to Pleistocene in area between Hsyning structure and Kaoping slope and its application for hydrocarbon exploration. Petroleum Geology of Taiwan 31.

Fuh, S.-C., Liang, S.-C., Wu, M.-S., 2003. Spatial and temporal evolution of the Plio-Pleistocene submarine canyons between Potzu and Tainan, Taiwan. Petroleum Geology of Taiwan 36, 1–18.

Galewsky, J., Silver, E.A., 1997. Tectonic controls on facies transitions in an oblique collision: the western Solomon Sea, Papua New Guinea. Geological Society of America Bulletin 109, 1266–1278.

Gani, M.R., Alam, M.M., 2004. Fluvial facies architecture in small-scale river systems in the Upper Dupi Tila Formation, northeast Bengal Basin, Bangladesh. Journal of Asian Earth Sciences 24, 225–236.

Graber, H.C., Beardsley, R.C., Grant, W.D., 1989. Storm-generated surface waves and sediment resuspension in the East China and Yellow seas. Journal of Physical Oceanography 19, 1039–1059.

Gupta, S., Allen, P.A., 2000. Implications of foreland paleotopography for stratigraphic development in the Eocene distal Alpine foreland basin. Geological Society of America Bulletin 112, 515–530.

Hjellbakk, A., 1997. Facies and fluvial architecture of a high-energy braided river: the Upper Proterozoic Seglodden Member, Varanger Peninsula, northern Norway. Sedimentary Geology 114, 131–161.

Ho, C.S., 1988. An Introduction to the Geology of Taiwan: Explanatory Text of the Geologic Map of Taiwan, second ed. Central Geological Survey, The Ministry of Economic Affairs, R.O.C. Taiwan.

Homewood, P., Allen, P., 1981. Wave-, tide-, and current-controlled sandbodies of Miocene Molasse, Western Switzerland. AAPG Bulletin 65, 2534–2545.

Hong, E., 1997. Evolution of pliocene to pleistocene sedimentary environments in an arc-continent collision zone: evidence from the analyses of lithofacies and ichnofacies in the SW foothills of Taiwan. Journal of Asian Earth Sciences 15, 381–392.

Hong, E., Huang, T.C., Yu, H.-S., 2004. Morphology and dynamic sedimentology in front of the retreating Tsengwen Delta, Southwestern Taiwan. Terrestrial, Atmospheric and Oceanic Sciences 15, 565–587.

Horng, C.-S., Shea, K.-S., 1996. Dating of the Plio-Pleistocene rapidly deposited sequence based on integrated magnet-biostratigraphy: a case study of the Madagida-Chi section, Coastal Range, Eastern Taiwan. Journal of the Geological Society of China 39, 31–58.

Horng, C.-S., Shea, K.-S., 2003. The Quaternary magnetobiostratigraphy of Taiwan and Penglai orogenic events. Ti-Chih, 51–83.

Hovikoski, J., Räsänen, M., Gingras, M., Roddaz, M., Brusset, S., Hermoza, W., Pittman, L.R., Lertola, K., 2005. Miocene semidiurnal tidal rhythmites in Madre de Dios, Peru. Geology 33, 177–180.

Hovikoski, J., Räsänen, M., Gingras, M., Ranzi, A., Melo, J., 2008. Tidal and seasonal controls in the formation of late Miocene inclined heterolithic stratification deposits, western Amazonian foreland basin. Sedimentology 55, 499–530.

Hu, C.-H., 1976. Studies on the Pliocene ostracodes from the Cholan Formation, Miaoli district, Taiwan. Proceedings of the Geological Society of China 19, 25–51.

Hu, C.-H., 1977. Studies on ostracodes from the Toukoshan Formation (Pleistocene), Miaoli district, Taiwan. Petroleum Geology of Taiwan 14, 181–217.

Hu, C.-H., Yang, L.-C., 1975. Studies on Pliocene ostracodes from the Chinshui Shale, Miaoli district, Taiwan. Proceedings of the Geological Society of China 18, 103–114.

Huang, T., 1967. Late Tertiary planktonic foraminifera from Southern Taiwan. The science reports of the Tohoku University. Second series. Geology 38, 165–192.

Huang, T.-C., 1976a. Neogene calcareous nannoplankton biostratigraphy viewed from the Chuhuankeng section, NW Taiwan. Proceedings of the Geological Society of China 19, 7–24.

Huang, T.-C., 1976b. Neogene clacareous nannoplankton biostratigraphy viewed from the Chuhuangkeng section, Northwestern Taiwan. Proceedings of the Geological Society of China 19, 7–24.

Huang, T., 1977. Late neogene planktonic foraminiferal biostratigraphy of the Tainan Foothills region, Tainan. Petroleum Geology of Taiwan 14, 121–145.
Huang, C.-S., 1984. Some planktic foraminifera from the olistostromes of the Kenting formation. Acta Geologica Taiwanica 22, 22–34.
Huang, C.-Y., 1986. Oligocene and Miocene stratigraphy of the Kuohsing area, Central Taiwan. Acta Geologica Taiwanica 24, 281–318.
Huang, T., Huang, T.-C., 1984. Neogene biostratigraphy of Taiwan. In: Ikebe, N., Tsuchi, R. (Eds.), Pacific Neogen Datum Planes: Contributions to Biostratigraphy and Chronology. University of Tokyo Press.
Jan, S., Wang, J., Chern, C.-S., Chao, S.-Y., 2002. Seasonal variation of the circulation in the Taiwan Strait. Journal of Marine Systems 35, 249–268.
Kao, S.-J., Jan, S., Hsu, S.-C., Lee, T.-Y., Dai, M., 2008. Sediment budget in the Taiwan Strait with high fluvial sediment inputs from mountainous rivers: new observations and synthesis. Terrestrial, Atmospheric and Oceanic Sciences 19, 525–546.
Komar, P.D., Miller, M.C., 1973. The threshold of sediment movement under oscillatory water waves. Journal of Sedimentary Petrology 43, 1101–1110.
Krassay, A.A., 1994. Storm features of siliciclastic shelf sedimentation in the mid-Cretaceous epeiric seaway of northern Australia. Sedimentary Geology 89, 241–264.
Ku, C.-Y., Sibuet, J.-C., Hsu, S.-K., Tsai, C.-H., 2009. The Neo-tectonic structure of the southwestern tip of the Okinawa Trough. Terrestrial, Atmospheric and Oceanic Sciences 20, 749–759.
Lee, P.J., 1963. Lithofacies of the Toukoshan-Cholan formation of western Taiwan. Proceedings of the Geological Society of China 6, 41–50.
Lee, T.-Q., Horng, C.-S., Kuo, C.-H., 1990. Magnetic fabric analysis of the plio-pleistocene series along the Tsengwenchi section, southern Taiwan and its tectonic implications. Proceedings of the Geological Society of China 33, 373–389.
Liew, P.-M., 1988. Quaternary stratigraphy in Western Taiwan: palynological correlation. Proceedings of the Geological Society of China 31, 169–180.
Lihou, J.C., Allen, P.A., 1996. Importance of inherited rift margin structures in the early North Alpine Foreland Basin, Switzerland. Basin Research 8, 425–442.
Lin, A.T., Watts, A.B., 2002. Origin of the West Taiwan basin by orogenic loading and flexure of a rifted continental margin. Journal of Geophysical Research 107, 2185.
Lin, M.-C., Juang, W.-J., Tsay, T.-K., 2001. Anomalous amplifications of semidiurnal tides along the western coast of Taiwan. Ocean Engineering 28, 1171–1198.
Lin, A.T., Watts, A.B., Hesselbo, S.P., 2003. Cenozoic stratigraphy and subsidence history of the South China Sea margin in the Taiwan region. Basin Research 15, 453–478.
Liu, Z., Tuo, S., Colin, C., Liu, J.T., Huang, C.-Y., Selvaraj, K., Chen, C.-T.A., Zhao, Y., Siringan, F.P., Boulay, S., Chen, Z., 2008. Detrital fine-grained sediment contribution from Taiwan to the northern South China Sea and its relation to regional ocean circulation. Marine Geology 255, 149–155.
Löwemark, L., Hong, E., 2006. Schaubcylindrichnus formosus isp. nov. in Miocene sandstones from northeastern Taiwan. Ichnos 13, 267–276.
MacEachern, J.A., Pemberton, S.G., 1992. Ichnological aspects of cretaceous shoreface successions and shoreface variability in the western interior seaway of north America. In: Pemberton, S.G. (Ed.), Applications of Ichnology to Petroleum Exploration. SEPM Core Workshop No. 17, Calgary.
MacEachern, J.A., Bann, K.L., Bhattacharya, J.P., Howell, C.D.J., 2005. Ichnology of deltas: organism responses to the dynamic interplay of rivers, waves, storms, and tides. In: Giosan, L. (Ed.), River Deltas – Concepts, Models and Examples. SEPM Special Publication, Tulsa, Oklahoma, p. 502.
Manighetti, B., Carter, L., 1999. Across-shelf sediment dispersal, Hauraki Gulf, New Zealand. Marine Geology 160, 271–300.
Meng, C.-Y., 1967. The structural development of the southern half of western Taiwan. Proceedings of the Geological Society of China 10, 77–82.
Miall, A.D., 1978. Lithofacies Types and Vertical Profil Models in Braided River Deposits: A Summary, Fluvial Sedimentology. Canadian Society of Petroleum Geologists, pp. 597–604.
Miall, A.D., 1996. The Geology of Fluvial Deposits: Sedimentary Facies, Basin Analysis, and Petroleum Geology. Springer.
Miller, D.J., Eriksson, K.A., 1997. Late Mississippian prodeltaic rhythmites in the Appalachian basin: a hierarchical record of tidal and climatic periodicities. Journal of Sedimentary Research 67, 653–660.
Miller, K.G., Mountain, G.S., Wright, J.D., Browning, J.V., 2011. A 180-million-year record of sea level and ice volume variations from continental margin and deep-sea isotopic records. Oceanography 24, 40–53.
Milliman, J.D., Kao, S.-J., 2005. Hyperpycnal discharge of fluvial sediment to the ocean: impact of super-Typhoon Herb (1996) on Taiwanese rivers. The Journal of Geology 113, 503–516.
Milliman, J.D., Lin, S.W., Kao, S.J., Liu, J.P., Liu, C.S., Chiu, J.K., Lin, Y.C., 2007. Short-term changes in seafloor character due to flood-derived hyperpycnal discharge: Typhoon Mindulle, Taiwan, July 2004. Geology 35, 779–782.
Mouthereau, F., Lacombe, O., 2006. Inversion of the Paleogene Chinese continental margin and thick-skinned deformation in the Western Foreland of Taiwan. Journal of Structural Geology 28, 1977–1993.
Mouthereau, F., Lacombe, O., Deffontaines, B., Angelier, J., Brusset, S., 2001. Deformation history of the southwestern Taiwan foreland thrust belt: insights from tectono-sedimentary analyses and balanced cross-sections. Tectonophysics 333, 293–322.
Pan, T.-S., 2011. A Study on Sedimentary Environments of Nanchuang Formation to Yangmei Formation Along the Dahan River Section, Northwestern Taiwan. Department of Earth Sciences, National Central University, Jhongli.
Pelletier, B., Stephan, J.F., 1986. Middle Miocene obduction and late Miocene beginning of collision registered in the Hengchun Peninsula: geodynamic implications for the evolution of Taiwan. Tectonophysics 125, 133–160.
Pemberton, S.G., MacEachern, J.A., Frey, R.W., 1992. Trace fossils facies models: environmental and allostratigraphic significance. In: Walker, R.G., James, N.P. (Eds.), Facies Models. Geological Association of Canada, pp. 47–71.
Pemberton, S.G., Spila, M., Pulham, A.J., Saunders, T., MacEachern, J.A., Robbins, D., Sinclair, I.K., 2001. Ichnology&Sedimentology of Shallow to Marginal Marine Systems: Ben Nevis&Avalon Reservoirs, Jeanne D'Arc Basin. Geological Association of Canada.
Pervesler, P., Uchmann, A., 2004. Ichnofossils from the type area of the Grund formation (Miocene, lower Badenian) in Northern lower Austria (Molasse Basin). Geologica Carpathica 55, 103–110.
Pollard, J.E., Goldring, R., Buck, S.G., 1993. Ichnofabrics containing Ophiomorpha: significance in shallow-water facies interpretation. Journal of the Geological Society, London 150, 149–164.
Prave, A.R., Duke, W.L., Slattery, W., 1996. A depositional model for storm- and tide-influenced prograding siliciclastic shorelines from the Middle Devonian of the central Appalachian foreland basin, USA. Sedimentology 43, 611–629.
Puigdefàbregas, C., Souquet, P., 1986. Tecto-sedimentary cycles and depositional sequences of the Mesozoic and Tertiary from the Pyrenees. Tectonophysics 129, 173–203.
Puigdefàbregas, C., Muñoz, J.A., Vergés, J., 1992. Thrusting and foreland basin evolution in the southern Pyrenees. In: McClay, K. (Ed.), Thrust Tectonics. Chapman & Hall, London, pp. 247–254.
Rahmani, R.A., 1988. Estuarine tidal channel and nearshore sedimentation of a late Cretaceous epicontinental sea. In: de Boer, P.L., Van Gelder, A., Nio, S.D. (Eds.), Tide-Influenced Sedimentary Environments and Facies. D. Riedel Publishing Company, Dordrecht, pp. 433–471.
Reading, H.G., Collinson, J.D., 1996. Clastic coasts. In: Reading, H.G. (Ed.), Sedimentary Environments: Processes, Facies and Stratigraphy. Blackwell Science, pp. 154–232.
Reijers, T.J.A., Mijnlieff, H.F., Pestman, P.J., Kouwe, W.F.P., 1993. Lithofacies and Their Interpretation: A Guide to Standardised Description of Sedimentary Deposits. Mededelingen Rijks Geologische Dienst, Haarlem, The Netherlands.
Savrda, C.E., Nanson, L.L., 2003. Ichnology of fair-weather and storm deposits in an Upper Cretaceous estuary (Eutaw Formation, western Georgia, USA). Paleogeography, Paleoclimatology, Paleoecology 202, 67–83.
Savrda, C.E., Uddin, A., 2005. Large Macaronichnus and Their Behavioral Implications (Cretaceous Eutaw Formation, Alabama, USA). Ichnos 12, 1–9.
Seno, T., Stein, S., Grip, A.E., 1993. A model for the motion of the Philippine Sea plate consistent with NUVEL-1 and geologic data. Journal of Geophysical Research 98 (B10), 941–948.
Shaw, C.-L., 1996. Stratigraphic correlation and isopach maps of the Western Taiwan Basin. Terrestrial, Atmospheric and Oceanic Sciences 7, 333–360.
Sibuet, J.-C., Hsu, S.-K., 1997. Geodynamics of the Taiwan arc-arc collision. Tectonophysics 274, 221–251.
Simoes, M., Avouac, P., 2006. Investigating the kinematics of mountain building in Taiwan from the spatiotemporal evolution of the foreland basin and western foothills. Journal of Geophysical Research 11.
Stephan, J.F., Blanchet, R., Rangin, C., Pelletier, B., Letouzey, J., Muller, C., 1986. Geodynamic evolution of the Taiwan-Luzon-Mindoro belt since the late Eocene. Tectonophysics 125, 245–268.
Suppe, J., 1980. A retrodeformable cross section of N Taiwan. Proceedings of the Geological Society of China 23, 46–55.
Suppe, J., 1981. Mechanics of mountain-building and metamorphism in Taiwan. Memoir of the Geological Society of China 4, 67–89.
Suppe, J., 1988. Tectonics of arc-continent collision on both sides of the south China sea: Taiwan and Mindoro. Acta Geologica Taiwanica 26, 1–18.
Tang, C.H., 1977. Late Miocene erosional unconformity on the subsurface Peikang high beneath the Chiayi-Yunlin coastal plain. Taiwan. Memoir of the Geological Society of China 2, 155–167.
Taylor, A.M., Goldring, R., 1993. Description and analysis of bioturbation and ichnofabric. Journal of the Geological Society, London 150, 141–148.
Teng, L.S., 1990. Geotectonic evolution of late Cenozoic arc-continent collision in Taiwan. Tectonophysics 183, 57–76.
Tensi, J., Mouthereau, F., Lacombe, O., 2006. Lithospheric bulge in the West Taiwan Basin. Basin Research 18, 277–299.
Tessier, B., 1993. Upper intertidal rhythmites in the Mont-Saint-Michel bay (NW France): perspectives for paleoreconstruction. Marine Geology 110, 355–367.
Thomas, R.G., Smith, D.G., Wood, J.M., Visser, J., Calverley-Range, E.A., Koster, E.H., 1987. Inclined heterolithic stratification-Terminology, description, interpretation and significance. Sedimentary Geology 53, 123–179.
Ting, H.-H., Huang, C.-Y., Wu, L.-C., 1991. Paleoenvironments of the late neogene sequences along the Nantzuhsien river, Southern Taiwan. Petroleum Geology of Taiwan 26, 121–149.
Walker, R.G., James, N.P., 1992. Facies Models: Response to Sea Level Change. Geological Association of Canada.
Walker, R.G., 2004. Facies Models: Responses to Sea Level Change, seventh ed. Geological Association of Canada, Toronto, Ontario.
Wang, Y., 1987. Continental margin rifting and cenozoic tectonics around Taiwan. Memoir of the Geological Society of China 9, 227–240.
Wang, C., 2004. Features of monsoon, typhoon and sea waves in the Taiwan Strait. Marine Georesources and Geotechnology 22, 133–150.
Wetzel, A., Uchmann, A., 1998. Biogenic Sedimentary Structures in Mudstones: An Overview, Shales and Mudstones, vol. I, Basin Studies, Sedimentology, and

Paleontology. E. Schweizerbart'sche Verlagsbuchhandlung, Stuttgart, Germany, p. 384.
Willis, B.J., Bhattacharya, J.P., Gabel, S.L., White, C.D., 1999. Architecture of a tide-influenced river delta in the Frontier Formation of central Wyoming, USA. Sedimentology 46, 667–688.
Wu, F.-T., 1968. Petrographic study of oil sands of Chunlun structure, Chiayi. Petroleum Geology of Taiwan 6, 183–195.
Wu, F.-T., 1970. Petrographic study of the sandstones in Kuantzuling area. Petroleum Geology of Taiwan 7, 229–241.
Wu, L.-C., Wang, Y., 1989. Depositional environments of the upper Miocene to lower Pleistocene series in the Yunshui-chi section, Chiayi area, Taiwan. Ti-Chih 9, 15–44.
Wu, C.-R., Chao, S.-Y., Hsu, C., 2007. Transient, seasonal and interannual variability of the Taiwan Strait current. Journal of Oceanography 63, 821–833.
Xu, K., Milliman, J.D., Li, A., Paul Liu, J., Kao, S.-J., Wan, S., 2009. Yangtze- and Taiwan-derived sediments on the inner shelf of East China Sea. Continental Shelf Research 29, 2240–2256.
Yeh, M.-G., Chang, Y.-L., 1991. The ichnofacies study of the Ailiaochiao formation, the Changchihkeng formation, Chiahsien-Meinung area, Kaohsiung. Petroleum Geology of Taiwan 26, 151–181.
Yeh, M.-G., Yang, C.-Y., 1994. Depositional environments of the upper Miocene to Pleistocene series in the Chungpu area, Chiayi, Taiwan. Petroleum Geology of Taiwan 29, 193–224.
Yu, H.-S., 1993. Contrasting tectonic style of a foredeep with a passive margin: Southwest Taiwan and South China. Petroleum Geology of Taiwan 28, 97–118.
Yu, H.-S., Chou, Y.-W., 2001. Characteristics and development of the flexural forebulge and basal unconformity of western Taiwan foreland Basin. Tectonophysics 333, 277–291.
Yu, H.-S., Hong, E., 2006. Shifting submarine canyons and development of a foreland basin in SW Taiwan: controls of foreland sedimentation and longitudinal sediment transport. Journal of Asian Earth Sciences 27, 922–932.
Yu, H.-S., Huang, Z.-Y., 2006. Intraslope Basin, seismic facies and sedimentary processes in the Kaoping Slope, Offshore Southwestern Taiwan. Terrestrial, Atmospheric and Oceanic Sciences 17, 659–677.
Yu, H.-S., Huang, Z.-Y., 2009. Morphotectonics and sedimentation in convergent margin basins: an example from juxtaposed marginal sea basin and foreland basin, Northern South China Sea. Tectonophysics 466, 241–254.
Yu, N.-T., Teng, L.S., Tai, P.-C., Yue, L.-F., 1999. Relative sea-level changes in Oligocene to Miocene strata in Northern Taiwan: a preliminary study. Journal of the Geological Society of China 42, 189–208.
Yu, N.-T., Teng, L.S., Chen, W.-S., Yen, I.-C., 2008. Facies characteristics of the upper-Neogene Nantzuhsienchi Section, Kaohsiung, SW Taiwan. Petroleum Geology of Taiwan 38, 30–56.
Zhang, G., 2002. Features of wind waves and their distribution in the sea area of the Taiwan Strait. Oceanic Bulletin 21 (in Chinese).